

Institut de Physique Nucleaire de Lyon

Master Internship

Simulations for a gamma-ray calorimeter (PARIS) based on new scintillators (LaBr3)

Author:
Xavier Fabian

Supervisor:
Dr. Olivier Stézowski

July 4, 2012

Remerciements

La fin de ce stage souligne non seulement la conclusion de 4 mois de travail de recherche, mais également de deux ans de master. Je procéderai donc dans un ordre chronologique.

Je voudrais d'abord remercier mes amis de Turbulence et du réseau de l'AFNEUS pour beaucoup de raisons, d'abord pour des discussions riches et surtout pour les liens de confiance et d'amitié que j'ai pu nouer. J'ai trouvé là des personnes d'une générosité inouïe et d'une dévotion parfois trop grande. Je ne vous nommerai pas par peur d'en oublier. Merci ensuite à mes collègues de M1 qui ont choisi un autre parcours que le mien, je pense surtout à Alex et Gaël avec qui j'ai partagé de très bons moments. J'ai aussi une pensée particulière pour Paul, Laura et Greg que je n'ai pas pu revoir cette année en stage, mais que j'ai beaucoup aimé côtoyer.

Je tiens maintenant à souligner que j'ai grandement apprécié partager la plupart de mon temps de cette année avec mes camarades de M2. Malgré la concurrence évidente qui devait arriver en fin d'année pour obtenir une bourse de thèse pour la plupart, nous nous sommes toujours serrés les coudes en nous entraidant lorsque l'un ou l'autre en avait besoin. J'ai eu la chance de cotoyer des futurs physiciens (ou autre, n'est-ce pas le saltimbanque ?) qui sont tous des personnes de grande qualité aujourd'hui et qui le seront encore davantage dans les années à venir, j'en suis convaincu. En vrac, je pense aux heures passées dans les deux bibliothèques à essayer de comprendre ce qui se passait dans nos UE, les cours de Guillaume sur le modèle standard ou les excitons, les moments de légèrté offerts par Nico et Bertrand (d'une manière très différente), les jeux de mots exceptionnels d'Alexis et Clément, les papilles gustatives chlorées de mon meilleur ami Arnaud, les débits de parole opposés de Cécile et Laura, le groupe facebook que vous animiez et qui m'a parfois sauvé la vie et j'en passe. Bref, merci d'avoir été là et d'avoir été vous. J'espère en revoir la majorité quand je repasserai à Lyon. Une note spéciale pour mon très cher ami Thierry, depuis maintenant longtemps, qui m'a plus aidé qu'il ne le croit.

Sur une autre note, j'aimerais désormais remercier le groupe de matière nucléaire, pour leur accueil aussi chaleureux que l'an dernier. Je pense particulièrement à Olivier qui, en plus de m'avoir accordé beaucoup de liberté dans mon travail, a rempli son rôle de maître de stage à merveille en prenant toujours le temps de répondre à mes questions (parfois plusieurs fois la même !) et en m'orientant lorsque j'étais un peu perdu. Merci aussi à l'appui que tu m'as donné auprès du groupe de Caen qui a contribué à me donner une chance pour poursuivre en thèse l'année prochaine, je ne l'oublierai pas. Je veux donc aussi remercier Camille, Daniel et Nadine pour leur temps lorsque j'étais bloqué et qu'Olivier était en déplacement. Je souhaite à Clément de profiter pleinement des trois années à venir dans ce groupe exceptionnel. Je ne peux évidemment pas négliger l'ensemble du personnel UCBL et IPNL que j'ai sollicité et qui ont été très efficaces lorsque j'en avais besoin.

En dernier lieu, je souhaite dire merci à mes parents. D'abord pour leur soutien permanent, mais aussi pour m'avoir encouragé, chacun à leur manière, à poursuivre dans la voie que j'ai choisie.

Contents

Introduction

From the end of the 19th century until now, mankind advances in the understanding of matter's structure and interaction with its environment has made a tremendous leap. Starting with the acceptance of quantum mechanics and relativity by the physicist community, followed by both experiments and theoretical models, we nowadays have a global model, named the Standard Model, to describe nature's fundamental particles and interactions that we henceforth confront with reality and constantly test.

This being said, we can choose a less elementary scale to work on as it is the case for nuclear physics where we are interested in the structure and behavior of the atomic nuclei. In order to test our comprehension on this topic, particle accelerators were constructed where the energy range we choose lets us see matter at a scale or another. In the case of nuclear physics, the energy range is centered around a few MeV per nucleon. Since we cannot look directly at the interactions inside nuclei, the preferred way to behold a nuclear process is to detect any emission radiated during one and try to explain the amount of each detected particles with our permanently evolving models.

For this to happen, we need more and more precise and performant detecting devices for we want to see increasingly finer effects. Because of the ressources needed for such devices and to augment our understanding of the involved interactions during detection, we compute simulated physics aiming to produce data and confront it with real measurements.

During my training course, I worked for the PARIS collaboration which is constructing a phoswich-type detector for SPIRAL2 based on new scintillators. We will see the details of this throughout this report, but a major aspect of my work was to study the scintillation light whereabouts and behavior inside the detector. The collaboration was motivated by the study of this facet, first, to better understand several experimental results, especially regarding the resolution degradation when optical-coupling between scintillators is achieved. Why is this effect worse for a specific scintillator than another ? Why is there a different detection inhomogeneity for different cristals ? These questions are not trivial and require thorough studies on the PARIS detector.

An important part of this work is the study of the neutron poisoning. We are in a specific gamma spectroscopy context and we thereby consider the neutrons as data pollution. Investigating their bearing could yield worthy information on how to discriminate them in an experiment. No work on the neutrons was done in this training course, still, it should be an essential part of any further study on this topic. This is particularly true with the upcoming measure campaign which will include neutron analysis.

This report is obviously first to be seen as a student work, neophyte in this field, but also as a part of the work described above. This document is divided in three sections. We will begin with a chapter setting a more specific context and reminding the fundamental physic's notions needed to work on the subject. This will be followed with a chapter on the detectors themselves, starting with a brief description of generic detector features and ending with a few scintillator specificities. We will finally describe and analyze our results in the last chapter.

Chapter 1

Physical Context

Before stepping right in the heart of the subject, it is important to present the environment in which we worked. Here, we will introduce the PARIS project through SPIRAL2 and we will remind the three γ-matter interaction processes.

1.1 Scientific Context

The availability of SPIRAL2 (Système de Production d'Ions Radioactifs en Ligne - génération 2)[1] in a near future opens the possibility of exploring new physics beyond our reach until then. With its capability for producing extreme density exotic beams (especially through neutron-rich beams), new regions of the *terra incognita* in the chart of nuclides will be reachable (see fig. 1.1). Although this project will allow to produce new physics, being able to observe it is another issue. One established solution to it is the usage of γ spectroscopy as a probe. Since the involved nuclear reactions will generate excited nuclei, the de-excitation γ-rays observation will yield precious information on the mechanisms of interest.

The Photon Array for studies with Radioactive Ion and Stable beams, commonly known as PARIS [2], is an international collaboration aiming to enhance present detection means, mainly to respond to the SPIRAL2 needs. The PARIS γ spectroscopy will use scintillator technology. More specifically, the accuracy requests of SPIRAL2 incited PARIS to use a new kind of scintillating material: the LaBr3. Its production is expensive and, for now, only cubic. This is why the collaboration decided to optically couple LaBr3 cubes with more conventionnal materials through the usage of phoswiches (more details in section 2.2.3).

The PARIS collaboration presented several physics cases to underline the γ spectroscopy usage suitability, for example the Jacobi shape transition study. A system undergoing a transition from oblate to triaxial and very elongated prolate while at high angular momenta is said to undergo a Jacobi shape transition. This transition is paired with the emission of a high-energy γ-ray characteristic of a GDR[2]. To fully describe it, one needs both the multiplicity and the energy sum of all gammas. Typically, for a GDR a high energy γ-ray is emitted (typically around 50 MeV), followed by a few others of about one MeV. The understanding of such a phenomenon will improve our knowledge of nuclei behavior in extreme conditions and more generally nuclear structure.

1.2 Theoretical reminders

Since our simulations are mainly on γ-rays detection, it is important to remember the γ-matter interaction processes [3]. Depending on the energy of the gamma of interest, one process among three will have the higher cross section. In order of increasing energy, we could be in the case of the photoelectric effect, the Compton scattering or the e^+e^- pair production. See figure 1.2 for each process occurrence likelihood.

[1] Second Generation System On-Line Production of Radioactive Ions
[2] Giant Dipole Resonance

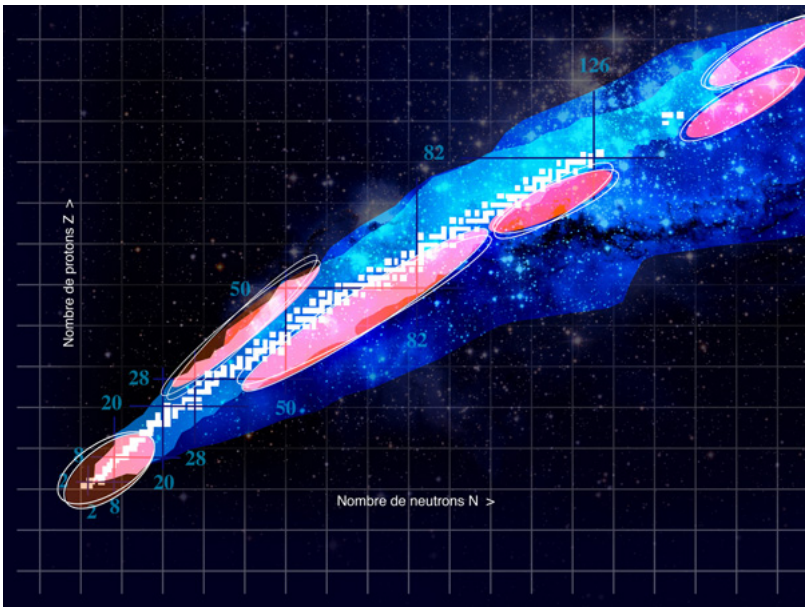

Figure 1.1: Chart of Nuclides

The coordinates (x,y) correspond to (neutron number, proton number). The light blue regions shows the already synthesized nuclei. In dark blue are never-observed predicted nuclei and in pink the nuclei potentially accessible through SPIRAL2. [1]

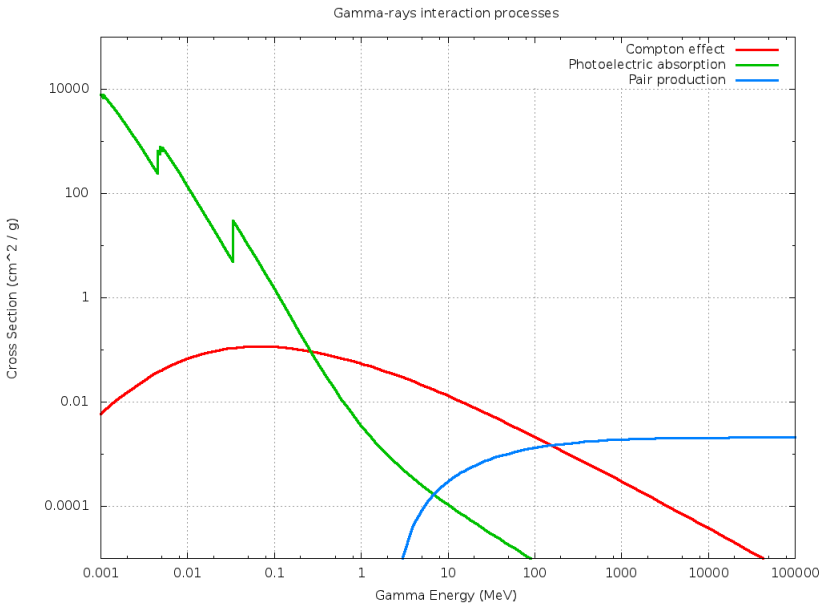

Figure 1.2: Three main processes of γ-matter interaction for NaI(Tl)

Cross section for each of the three γ-matter interaction processes plotted against the incident γ-ray energy for a NaI(Tl) crystal. We can clearly see the dominance of the photoelectric effect at low energies (below 0.2 MeV) and of the pair production at high energies (over 200 MeV). Between 0.2 MeV and 200 MeV, the Compton effect prevails. [4]

1.2.1 Photoelectric Effect

This process, dominant at very low energy, is the complete absorption of the incident photon by a given atom. The absorbed energy is transfered to one of the atom's electron and, if the photon energy is greater than the ionization energy, the electron is ejected from the atom. By energy conservation, the kinetic energy of this photoelectron is $E_K = h\nu_\gamma - E_{ionization}$, where ν_γ is the incident photon frequency.

1.2.2 Compton Scattering

While in the photoelectric effect the photon acts as a wave, in the Compton scattering one must consider the photon a body. In fact, this effect is nothing more than an inelastic scattering between the incident photon and an electron. A fraction of the photon's momentum is transferred to the scattering electron, possibly triggering ionization, and its wavelength's shift is given by:

$$\lambda_1 - \lambda_0 = \frac{h(1 - cos(\theta))}{m_e c} \tag{1.2.1}$$

Where:

- λ_0 and λ_1 are respectively the wavelengths of the incident and scattered photons.
- θ is the angle between the scattered photon and the scattering electron.

This effect implies difficulties for the full detection of an incident γ-ray. Indeed, with a wide range of possible energy deposit and several probable interaction point inside and outside the detector, the γ-ray energy reconstruction is not an easy task, although solutions exist. For example, the usage of detector clusters decreases the loss due to side leak.

1.2.3 Pair Production

When a γ-ray has sufficient energy, it may materialize in an electron-positron pair. Since both masses are equal to 511 keV, the energy threshold for the pair production process is 1.022 MeV. Note that such a process cannot occur in void. We can always use the centre of mass frame for an electron-positron pair where the total momentum is set to zero. Since the energy of a photon is given by the relativistic equation $E_\gamma^2 = m_\gamma^2 c^4 + p_\gamma^2 c^2$ and $m_\gamma = 0$, implying $E_\gamma = p_\gamma$ ($c = 1$), we cannot have a zero-momentum photon, which would be the case in the annihilation of an electron-positron pair yielding only one photon (by time reversal, we fall back on the materialization of the photon). Such a process requires a fourth body in order to respect momentum conservation which may be found in the neighborhood of a nucleus.

Chapter 2

Detectors

My internship was about the characterization of a specific detector, thus, it is necessary to define several concepts. We will first discuss of generic features any detector may have, including PARIS. Then, we will focus on a precise detector type: the inorganic scintillators, where we will describe a little bit theory on the scintillation process, some unique aspects of scintillation detection and the physical assemblies used for experiments.

2.1 General characteristics

We commonly characterize a detector by establishing standard figures. This allows a comparison between them, enabling an enlightened choice for a specifc physics case. In my training course, I focused on the efficiencies and the resolution measurement.

2.1.1 Efficiencies

The first aspect studied for a given detector is its efficiency [5] [6], or should we say its efficiencies since several types are in use. The main idea stays the same for each: how capable and adequate is the utilized detector for a given physics case ? Here, "detected" will have the sense of "interacted at least once". This specification is important since we need to account for the Compton effect, involving that a given incident γ-ray is not always **fully** detected.

It is also important to note that the efficiencies depend on the nature and the energy of the incident particle. Obviously, the interaction processes with matter for a neutron or a photon are not the same and the cross section of these different processes depends on the energy of the particle.

Intrinsic

The intrinsic efficiency is defined as the fraction of detected particles over the number of particles entering the detector:

$$\epsilon_{intr} = \frac{N_{detected}}{N_{entering\ detector}} \tag{2.1.1}$$

In a way, it could be seen as the "opacity" of the detector, an "opacity" equal to one means that each entering particle interacts at least once with it.

Absolute

The absolute efficiency is the number of detected particles over the number of emitted particles:

$$\epsilon_{abs} = \frac{N_{detected}}{N_{emitted}} = \epsilon_{intr}\epsilon_{geom} \tag{2.1.2}$$

In practice, this is done by placing the detector of interest near a source of known activity and

just wait for it to count. The number of hits depends on the distance between the detector and the source and on the facing angle of the detector. In fact, the absolute efficiency may be defined as the product between the intrinsic efficiency (ϵ_{intr}) and the geometrical efficiency (ϵ_{geom}), the former being defined above and the latter being the solid angle fraction subtended by the detector.

Photopeak

The photopeak efficiency follows the same idea than the absolute efficiency, except that the incident particle must be fully absorbed (thus be in the correct peak). This quantity is useful to appraise the number of particles correctly detected (e.g. Compton Scattering issues for γ-rays).

$$\epsilon_{pp} = \frac{N_{pp}}{N_{emitted}} \tag{2.1.3}$$

Peak on total

The "peak on total" is the ratio of correctly detected particles versus detected particles:

$$\epsilon_{p/T} = \frac{N_{pp}}{N_{detected}} = \frac{\epsilon_{pp}}{\epsilon_{abs}} \tag{2.1.4}$$

It is mathematically quite simple: we only need to divide the photopeak efficiency by the absolute efficiency. This yields a percentage indicating how much of the detected particles are fully detected.

2.1.2 Resolution

The resolution is a way to quantify how accurate the detected energy value is measured [6]. Even in an ideal case where an incident γ-ray is fully absorbed, a real detector won't necessarily return its exact energy. It is always more or less a certain value: the resolution. Because we want to be as precise as possible in our measurements, we will always foster a small resolution detector. While we now have the concept of the resolution, its mathematical definition depends on the accepted norm in a given context (taking into account the possible misnomers). Let's define ours.

Whenever a γ-ray is detected, it belongs to a gaussian-shaped peak in the spectrum. Let us recall the gaussian formula:

$$g(x) = Aexp\left(- \frac{(x - x_0)^2}{2\sigma^2} \right) \tag{2.1.5}$$

With:

- A the peak height;
- x_0 the peak centre;
- σ being related to the peak width.

Now, with a suitable fit on a given spectrum we are able to find all these parameters. Obviously, we will use σ to extract the resolution. We define:

$$\Delta E = FWHM^1 \tag{2.1.6}$$

Knowing that:

$$FWHM = 2\ ln(2\sqrt{2})\sigma \tag{2.1.7}$$

[1] Full Width at Half Maximum

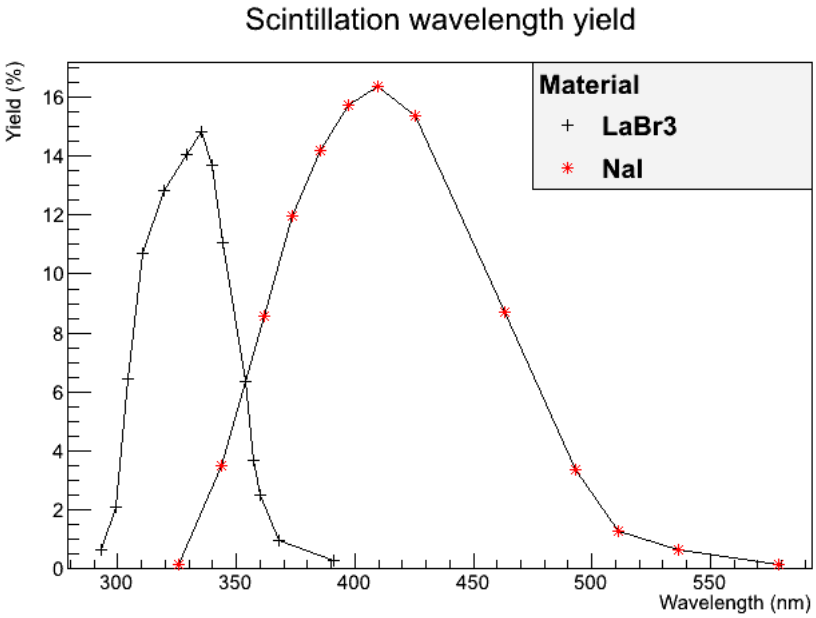

Figure 2.1: Scintillation photons wavelengths
Although the LaBr3 and the NaI both emit near the visible region on the UV edge, the peak is near 420 nm for the NaI and 340 nm for the LaBr3. Data taken on St-Gobain website [7] and Melcher's article [8].

In our context we will call "resolution" the relative resolution and define it the following way:

$$Resolution = \frac{\Delta E}{E}(\%) \tag{2.1.8}$$

As an exemple, our benchmark will be the LaBr3 scintillator with a resolution of 3% at 662 keV.

2.2 Scintillators

Scintillators are specific materials sharing a common property: photoluminescence. When struck by a particle and through a process called scintillation, a scintillator reemits photons with a material-dependent distribution for their wavelengths (see fig. 2.1). Of course, we are only interested in materials as much transparent as possible to their own and their neighbor's scintillation light. Indeed, the principle of a scintillation detector is to count the number of reemitted photons: the higher the energy of the incident particle, the higher the number of photoluminescent photons.

There is a temperature dependance on the scintillation light yield. For example, Amsler *et al.* [10] show that a pure CsI crystal's yield operating at room temperature is 3200 ± 400 photons/MeV, while at liquid nitrogen temperature (77 K) the same crystal emits 50000 ± 5000 photons/MeV. This last yield is comparable to Thallium activated CsI at room temperature. This is explainable by the number of electrons trapped in specific impurity centres where the probability to return to a possible luminescence centre depends on the thermal excitation of the crystal lattice as we will discuss in the next section.

Different kind of scintillators exist. They differ both by the nature of their material (thus the subsequent scintillation processes) and by their characteristics (see table 2.1). We can differentiate two major categories: organic and inorganic scintillators. We will not speak much of the former for we will focus on the latter type which we used. For the inorganic ones, the scintillation is a property of the

scintillator composition	density (g/cm^3)	index of refraction	wavelength of maximum emission (nm)	decay time constant 1/e (ns)	scintillation pulse height[1]	notes
NaI	3.67	1.78	303	60	190	2)
NaI(Tl)	3.67	1.85	410	250	100	3)
CsI	4.51	1.95	310	10	6	3)
CsI(Tl)	4.51	1.79	565	1000	45	3)
CsI(Na)	4.51	1.84	420	630	85	3)
^{6}LiI(Eu)	4.06	1.96	470-485	1400	35	3)
CaF_2(Eu)	3.19	1.44	435	900	50	
BaF_2	4.88	1.49	190/220 310	0.6 630	5 15	
BGO	7.13	2.15	480	300	10	
$ZnWO_4$	7.87	2.2	480	5000	26	
$CdWO_4$	7.90	2.3	540	5000	40	
$PbWO_4$	8.28	2.16	480	2/7/26	0.8	
CsF	4.65	1.48	390	5	5	3)
CeF_3	6.16	1.68	300 340	5 20	5	
LSO	7.40	1.81	420	42	75	
GSO	6.71	1.9	440	60	20	
YSO	4.45	1.8	420	35	50	
YAP	5.50	1.9	370	30	40	
ZnS(Ag)	4.09	2.35	450	200	150	4)
ZnO(Ga)	5.61	2.02	385	0.4	40	4)

[1] relative to NaI(Tl) [2] at 80 K [3] hygroscopic [4]polycrystalline

Table 2.1: Physical properties of various commercial scintillators [9]

crystalline structure of the material[2], while it is molecular in nature for the organic scintillators. This implies that in our inorganic case, we need to be in a solid state. This is an important constraint, particularly for our hygroscopic[3] crystals [11]. More specifically, we used LaBr3, CsI(Tl) and NaI(Tl) crystals throughout this work.

In this section, we will speak of the process causing scintillation (from incident particle interaction to luminescence), the emitted signal shape and the real assemblies for the experimental devices.

2.2.1 Scintillation Process

For scintillation light to be produced several steps must be taken [6] [11] [9] [12]. An incident particle may interact with a scintillator via multiple processes, their likelihood being related to the initial energy. Focusing on γ-rays, we still expect a generic sequence for subprocesses. Here is a non-exhaustive summary of it:

1. A γ-ray enters the scintillating material and interacts once or several times with the present matter. The deposited energy at a given point is between 0% and 100% of the incident energy (more probable percentages depending on the involved process - see section 1.2). In the case of pair creation and through annihilation with present electrons, we will observe the genesis of new γ-rays which will act as new incident particles (return to step 1 for each of them - avalanche !);
2. On each interaction point, an electron will gain access to the conduction band and create a hole in the valence band. Eventually, this pair may bind in an exciton and occupy an energy state on the exciton band (see figure 2.2a). A few mechanisms may follow:
    - *Deep electrons* coming from a low orbital in a given atom will induce a reorganisation of the electron cloud, resulting in the emission of photons, mostly X-rays, for each electron energy level change (return to step 1 for each photon - avalanche !). The deep electron itself will then act as one of the two below.
    - *Low energy electrons* reaching impurity centres[4] will more likely de-excite following three possibilities: quenching, trapping or luminescence (see below). It has been shown that excitons are the main responsible for luminescence in our case (Alkali crystals, Thallium doped) [11].
    - *High energy electrons* can follow the low energy electrons' sequence and/or act as an incident particle (return to point 1 - avalanche !).

At the end of each avalanche, we expect to fall on low energy electron/hole pairs. Depending on the impurity centre type they reach, an electron or an exciton will de-excite through (see figure 2.2b):

- *Quenching*: Radiationless thermal dissipation;
- *Trapping*: Fall in a metastable level resulting in either a radiationless thermal dissipation or a return to the conduction/exciton band by gaining energy from the lattice's thermal vibrations;
- *Luminescence*: The scintillation light emission we are interested in.

Although we focused on γ-rays, note that the scintillation process is similar for each incident particle. What changes is the initial interaction process with matter.

In Melcher's article [8], we can find a formula for the overall efficiency of the conversion process from the incident particle to scintillation light:

$$\eta = \beta S Q \tag{2.2.1}$$

where:

[2] Although there exists a few exceptions... [11]
[3] Characteristic where a crystal liquefy when in contact with water, including air moisture.
[4] We used Thallium doped crystals.

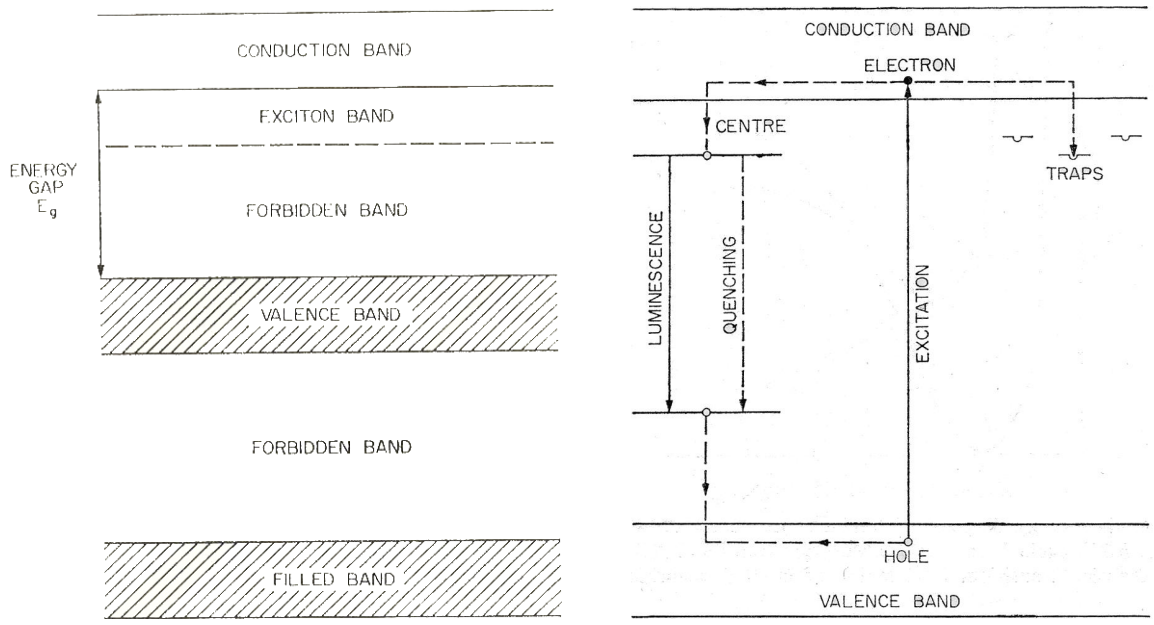

Figure 2.2: Energy bands and impurity centres of inorganic scintillators
On the left, we see a classic band diagram with an exciton band. An important point is the energy gap size: it is only a few eVs so that any impigement will most likely create an electron/hole pair (move an electron to the conduction band while leaving a hole behind in the valence band). On the right, another energy band diagram. This time, it is the impurity centres one where we can see the different de-excitation modes. Both figures are taken from Birks' book [11].

- β is the conversion efficiency of the incident γ-rays to electron/hole pairs. It can be calculated from the physical properties of the material with a reasonable confidence;
- S is the proportion of electron/hole pairs which will ultimatly de-excite through luminescence. As of year 2000, no model existed to calculate accurately S. This is the difficult variable to reach, but it can be deduced from the two others;
- Q is the quantum efficiency of the luminescence centres. It is possible to bypass both β and S to measure directly Q through UV excitation of the luminescence centres themselves.

It is not an easy task for an incident particle to be converted to scintillation light, especially because of all the possible subprocesses where a part of the incident energy is lost. This is not a problem though since the mean number of luminescent photons remains the same, following a gaussian law. However, it does imply that we need a high statistic to be able to conclude on the physics case we are studying. Otherwise, we will be hindered by many other difficulties between the scintillation light emission and its final detection as we will later show.

2.2.2 Signal

The scintillation signal reaching the end of the scintillator (entering the photocathode) is very specific. The most general spectrum of a scintillating signal shows three parts, in time order: a rise time, a fast component and a slow component. The rise time, usually very short, is followed by a fast exponential decay and a slow one [6]. This is rather general because in some material there is only one component (true for the LaBr3) while in others, a third component has been observed [10]. The general form is therefore written as:

$$N = A\ exp\left(\frac{-t}{\tau_f}\right) + B\ exp\left(\frac{-t}{\tau_s}\right) \tag{2.2.2}$$

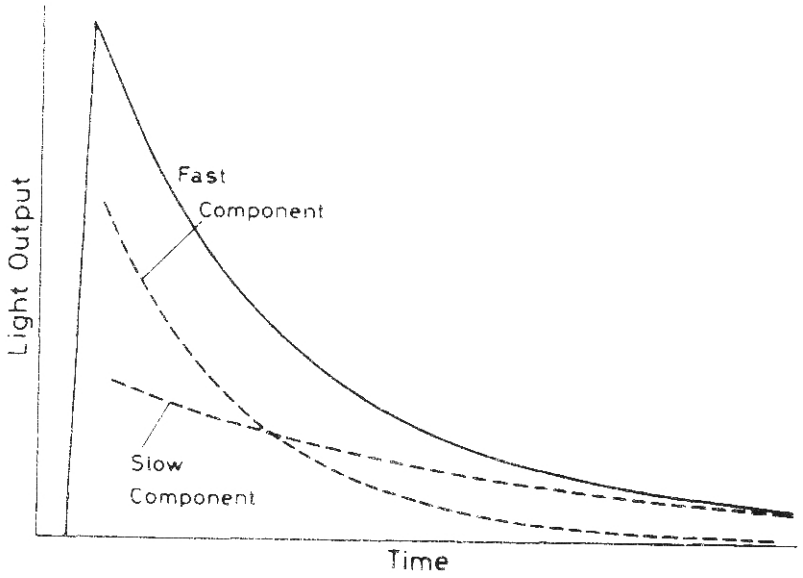

Figure 2.3: General shape of a scintillating signal [6]

where τ_f and τ_s are respectively the fast and slow decay constants. The magnitudes A and B depend on the used material, although A is generally higher than B (see figure 2.3).

The scintillating process described in 2.2.1 may explain the existence of several components. When an exciton reaches a trapping centre it becomes stuck in a metastable level characteristic of the doping material. If it captures enough thermal vibration from the lattice, it may return to the conduction band and eventually reach a luminescence centre. A metastable level thereby has a specific lifetime due to the scintillating material, the doping material and the temperature of the lattice. This suggests that each exponential component found in the signal could be linked to one or more metastable level lifetime, allowing the existence of numerous components.

The reason why we are interested in the signal analysis is that we may learn something on the interaction point or depth. This would be particularly useful for Compton γ-rays reconstruction for a cluster assembly.

2.2.3 Physical assembly

Because of the hygroscopic property of the inorganic scintillators we used, we need to isolate them from any moist air with an aluminium casing. Saint-Gobain Corporation grows the needed crystals and assemble them in the required casing. PARIS recently had a problem with one of its LaBr3 scintillator which unexpectedly started to show yellow spots. This might be due to the recycled aluminimum used to weld. Since it is less pure and a little more porous than freshly aluminimum made from ore, it is possible that moist air got inside and partially melted the LaBr3. The issue was addressed and should be resolved.

The aluminium casing surrounds the scintillating material (materials in the case of a phoswich - see below) and is coated with a reflector on the interior face to direct the scintillation light toward the photocathode. The rear side is not covered with the casing, it is instead coupled to a photomultiplier through a window.

Another point is that for some details we have to work with a *black box*. Indeed, Saint-Gobain keeps industrial secrets. For example, they informed us that the internal reflectors could be considered fully Lambertian in a first approximation and we do not know anything about the interface between the two scintillators in the case of a phoswich.

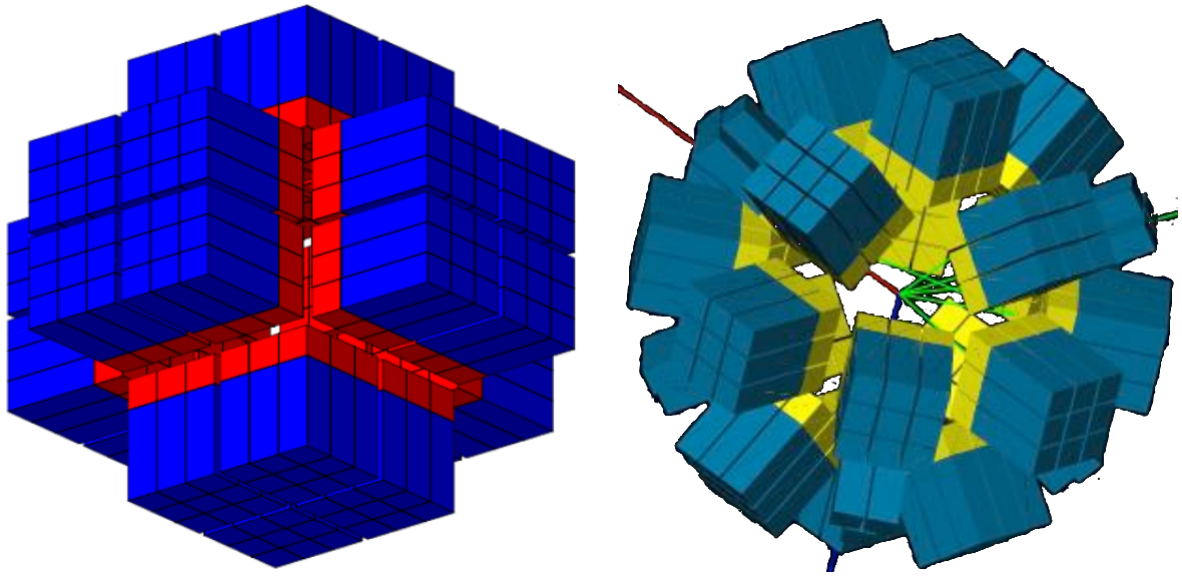

(a) (b)

Figure 2.4: Proposed PARIS array geometries
Since the LaBr3 crystals can only be built on cubes (until recently), several geometries are being tested to construct a final 4π array. On the left, a cubic geometry and on the right, a more spherical one. Both configurations have been studied by the PARIS collaboration [2].

While in this work we studied only isolated detectors, the final PARIS array will be a 4π detector. The used cluster assemblies will be made of several phoswiches (3 X 3) and the array itself will be made of several clusters. An important part of PARIS' work is to focus on γ-ray reconstruction for Compton scattering in a cluster, where an incident γ-ray interacts at several points. See figure 2.4.

Reflectors

As we said, the interior face of the casing is coated with a reflector. Its properties influence the scintillation light detection in many ways, as we will discuss in chapter 3. The basic model for a reflector is the one following Snell-Descartes laws which we call *Specular*. Another model, mostly used today with Teflon coating, is the one we call *Lambertian*. This one reflects incident light in 2π. In reality, we need to consider several components for the real interaction process between an incident luminescent photon and the reflecting surface. In most cases, a surface will behave both as a Lambertian and a Specular reflector, among others. In GEANT4, where all our simulations where done, the UNIFIED model [13] implements a realistic reflection with several parameters. Let us summarize it.

The first important part of the UNIFIED model is the surface shape, which is made of *micro-facets* in the most general case. One of the parameters, α, describes the shape of the micro-facets for it is the angle between the surface normal and a given micro-facet (see figure 2.5). α belongs to gaussian distribution of standard deviation σ_α. Of course, we also define the optical indexes for each side of the reflecting surface. We then have four constants defining the direction toward which an incident photon will be reflected, their sum being equal to 1 since they are probabilities. On the figure, they are named $C_{bs}R$, $C_{ss}R$, $C_{sl}R$ and $C_{dl}R$:

- $C_{bs}R$ is the backscattering spike constant where an incident photon reflects toward its incident axis;
- $C_{ss}R$ is the Specular spike constant describing the reflection about the average normal of the surface (what we call here *Specular*). θ_i and θ_r are the incidence/reflection and the transmission angle in this case;

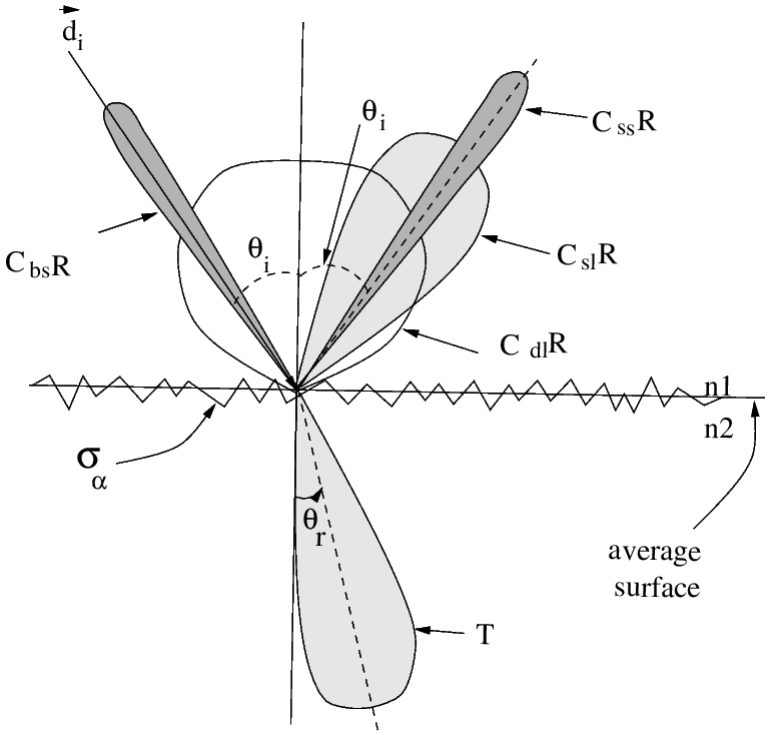

Figure 2.5: The UNIFIED model's surface and reflection (See 2.2.3 for the discussion. Taken from Levin *et al.* [13].)

- $C_{sl}R$ is the Specular lobe constant describing the reflection about the normal of a micro-facet (randomized in accordance with α when the impact occurs);
- $C_{dl}R$ is the diffuse lobe constant or the Lambertian reflection probability.

The model is quite more complex with the implementation of realism control as an example. Because of the numerous randomizations throughout the reflection process, it happens that an incident photon is about to follow an unrealistic path after the calculations. This is prevented with internal mechanisms.

Phoswich

A phoswich[5] assembly (PW) is nothing more than two opticaly-coupled scintillators with a common photomultiplier. The reason why the PARIS collaboration decided to use such devices is that the LaBr3 is an expensive crystal and its only-cubic shape does not have enough depth to entirely absorb high-energy particles. While the high performance of the LaBr3 is now well-known, numerous questions arise when it comes to couple it with lower resolution (both in time and energy) scintillators (CsI(Tl) and NaI(Tl)). CsI and NaI crystals were selected especially because of their transparency to the LaBr3 scintillating light.

Although the optical-coupling between a LaBr3 and a NaI or CsI crystal degrades the resolution comparing to a stand-alone LaBr3 cube, the full absorption of incident particle is higher. Having two different scintillating materials also presents another asset which is the access to more information on the detection point location as we discussed in the last section.

[5]Comes from "Phosphor sandwiches" according to St-Gobain website [7]

Chapter 3

Simulations

The PARIS collaboration has developed a specific package in the GEANT4 and ROOT environments to simulate the required physics cases. All the work reported here was done using this package in which I have implemented new geometries and analysis procedures.

In GEANT4, each particle is a specific object. For example, the scintillator emits "optical photons" when struck by a particle which are not the same as "gamma" particles, although both are photons in reality. The optical photons are sensible to optical properties attached to specific regions of the simulations, for example the optical index changes between two media, which is not the case for gammas. It is useful to do preliminary analysis for we can deactivate optical photon creation (thus lowering needed computing time) and work directly with γ-ray energy deposit. Despite the access to this information is not realistic, in our case it is accessible and it allows us to perform preliminary analysis on how the scintillators' signal is generated.

The main issue (or not) with simulations is the perfectness of the results. In reality, when a γ-ray is detected, we don't have any information on it before a lot of steps are done (e.g. γ-ray physical interaction with matter through one of the three main processes, complex crystal reaction to it, release of scintillating photons and traveling through the crystal with probable reflection or absorption on the border, reaching of the entrance of the photocathode with any luck, followed by the photomultiplier electron cascade and the quantum loss during the process, the electronic signal treatement beginning...). In computer generated physics, we control everything and we have access to all information at any time. For example, the used ROOT datatree was made of four branches each containing detailed information on the incident particle, on the hits (interaction points in the scintillator) and on both the beginning and the end of each optical photon trace. Consequently, we need to introduce biasis in our results in order to better reproduce reality. For instance, when looking at the γ-ray energy deposit in the photopeak region, we have a full absorption. For a monoenergetic source, this numericaly appears as a perfect peak, while in reality its width should not be zero. This is why in our preliminary analysis, we enabled a gaussian smearing on the detected energy.

The point here is to emphasize that we need to carefuly choose which process we have to perform or to introduce in the data creation sequence or in its analysis to make it as useful and realistic as possible or needed.

Of course, all our simulations are to be confronted with experimental data to come. A measure campaign is scheduled soon and any discrepancy between the real and the simulated experiences will need to be subject to a more thorough study. Indeed, it will point to unexpected, misunderstood or error sources which need to be clarified before constructing a complete experimental 4π array.

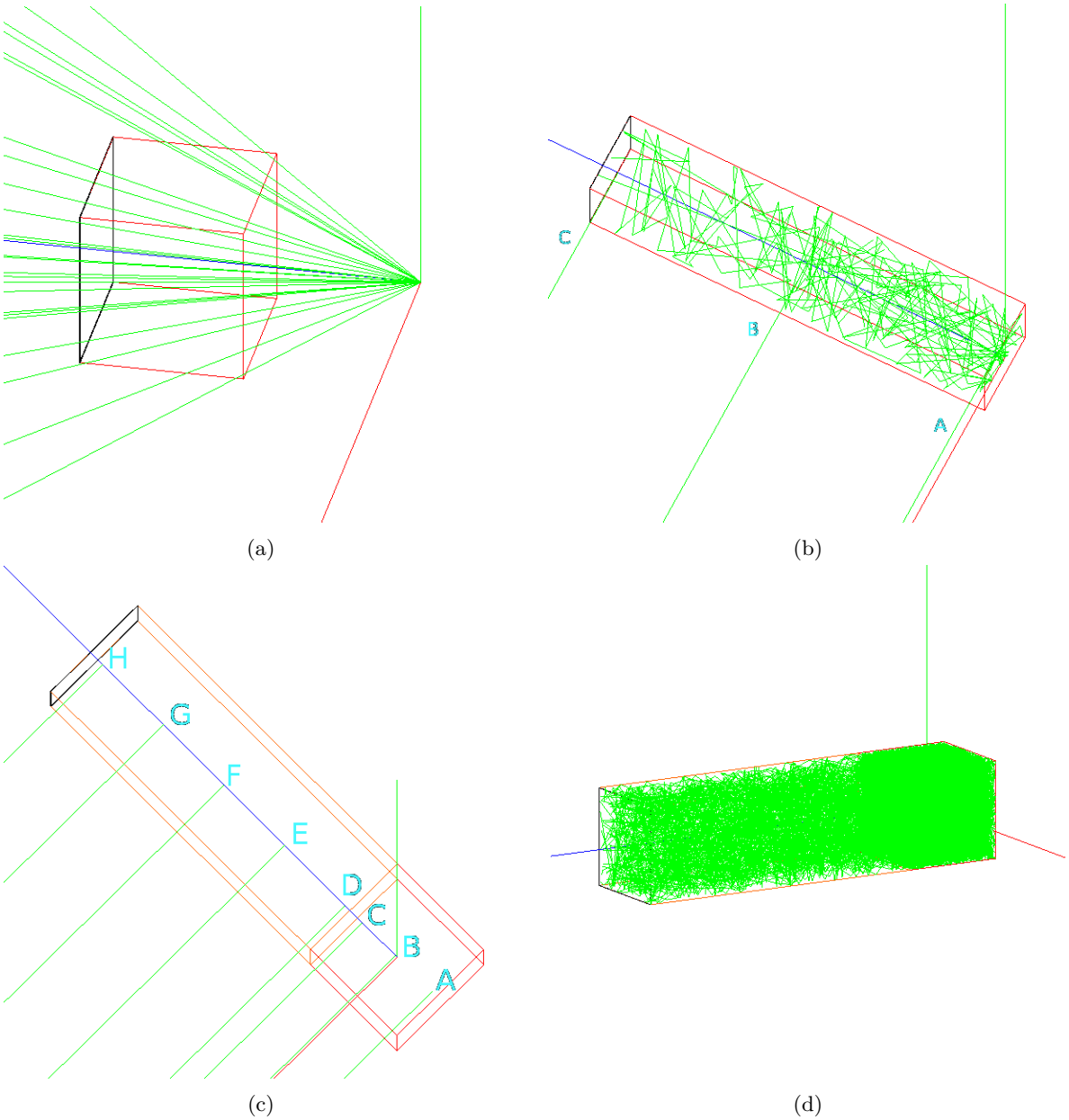

(a) (b) (c) (d)

Figure 3.1: Utilized assemblies and sources

- The **top-left figure** is a Basic cube with the photocathode represented as the black square on its rear. Starting at the origin, we can see a cone beam (the green lines are γ-ray tracks).
- On the **top-right figure**, we have the Basic cuboid. We can see the optical photons tracks being reflected inside the detector with a γ-ray source near the origin inside the cuboid (source A). The optical photons end their course after several reflections when they reach the photocathode. The three labelled green lines are geantinos (abstract particle of GEANT4 with no interaction whatsoever) emitted from the used sources in the scanning configuration. The sources emit geantinos for the illustration, but in our simulation this configuration corresponds to 30 keV γ-rays which were immediately absorbed.
- The **bottom-left figure** is a NaI phoswich. The green lines origin are the eight sources, also labelled, inside the detector for the scanning configuration.
- The **bottom-right figure** is the same phoswich, but with the green lines being optical photons. We clearly see a higher density in the LaBr3 where the source is (source B). This trapping effect will be discussed in section 3.2.3.

For more information on the sources, see section 3.2 introduction text.

3.1 Models

In order to work with a full scintillator, we need to define specific components which we will later assemble. For the sake of clarity, it is important to notice that our geometries had both x-axis and y-axis symmetries. All the peculiarities were along the z axis.

3.1.1 Components

The environment was defined as "pseudo-air", meaning an almost γ-ray transparent medium and a perfect absorber for optical photons. This allows the usage of a γ-ray source while forbidding any optical photons loss (escape to infinity). If a given optical photon was absorbed in that pseudo-air, it was accounted for and labeled as such, allowing selection in data processing. These four elements are the basic parts of the assemblies we worked on:

- **Cube**: The "Cube" will refer to a 2" cube made of LaBr3. The real LaBr3 scintillators produced at St-Gobain are of that shape.
- **Cuboid**: The "Cuboid" is a 2" $\times$ 2" $\times$ (6" *or* 10") cuboid made of LaBr3, NaI or CsI.
- **Photocathode**: The "Photocathode" is a $2,54 \times 2,54 \times 0.02\ cm^3$ pseudo-aluminium (perfect absorber, perfect quantum efficiency[1]) block. Throughout our work, an optical photon reaching the photocathode will be considered detected.
- **Reflector**: The "Reflector" is the material at the border between the scintillator and the pseudo-air. Depending on its definition, an incident optical photon will follow different reflection patterns. They had a reflectivity of 97%. As we discussed in section 2.2.3, we used GEANT4's implementation of the UNIFIED model. Our reflectors were either fully Specular (Specular spike constant = 1) or fully Lambertian (diffuse lobe constant = 1) (see figure 3.2), with both the Specular lobe and the backscattering constants equal to 0.

The scintillation crystals had the following caracteristics (data taken in Stézowski's HDR [14] and the refractive index online database [15]):

	Scintillation yield (photons/MeV)	Optical index (at wavelength λ)
LaBr3	63 000	2.05 ($\lambda = 380\ nm$)
NaI	38 000	1.85 ($\lambda = 370\ nm$)
CsI	38 000	1.78 ($\lambda = 650\ nm$)

Note that the real CsI yield is 54 000 photons/MeV, but we wanted to compare only the optical index change effect between the NaI and the CsI.

3.1.2 Assemblies

Now that we have our basic bricks, we can assemble them in detectors. We used five different configurations (see figure 3.1).

- **Basic cube**: a Cube coupled with a Photocathode (highest z side) and Reflectors on all faces (except the Photocathode's one).
- **Basic cuboid**: a 10" LaBr3 Cuboid coupled with a Photocathode (highest z side) and Reflectors on all faces (except the Photocathode one).
- **3 X Phoswiches**: a Cube as the entry face, followed by a 6" Cuboid (LaBr3, NaI or CsI) and a Photocathode at the end. There are Reflectors on all faces, except at the Photocathode one and at the boundary between the Cube and the Cuboid.

[1] The quantum efficiency is the probability for an absorbed photon to yield an electron. It does not exceed roughly 30%. This was simulated using material having 30% of the true optical photon yield, thus saving computing time.

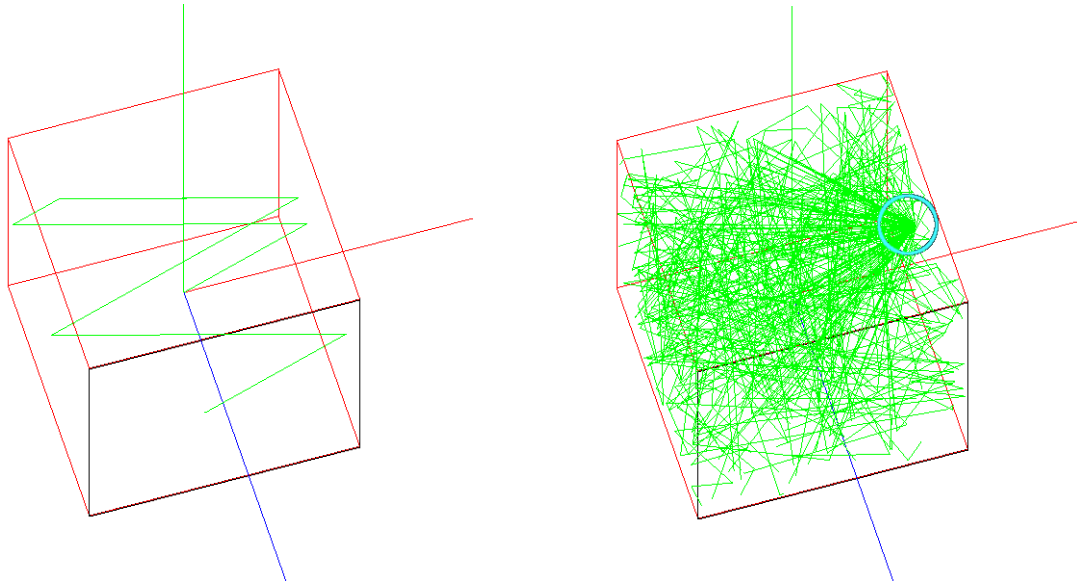

(a) (b)

Figure 3.2: Reflectors
In both cases, 100 optical photons (green tracks) were shot from the origin at the same angle. On the left side, all the photons followed the same path ; the reflector is Specular. On the right side, the first reflection point is circled in cyan. We see the effect of the Lambertian surface as the 100 optical photons were reflected within 2π.

3.2 Gamma spectroscopy

In order to simulate different beams, we used GEANT4's GPS[2]. We worked with two source configurations: large beams and scanning.

Large beams

For the preliminary tests and for the efficiencies, the source was 5 cm apart from the detector and the γ-rays' energies were either a continuum between 0 and 50 MeV or several characteristic discrete energies[3]. In both cases, we either shot in 4π or in a cone toward the detector entry face.

Scanning

The optical characterization was performed through a scanning of the detector with two energies (30 keV and 662 keV) for the incident γ-rays. The 30 keV sources were placed in the middle of the detector and were distributed along its axis (z). This is a way to force local energy deposit. The 662 keV sources were also distributed along the detector's axis, but outside of it, on the negative x side. This last one corresponds to real collimated sources and the experimental data we compare to were produced using this technique (using a ^{137}Cs source). For both energies, the γ-ray was emitted in the x direction. Again, for the sake of clarity, we introduced specific alphabetical labels starting at the lowest z to differentiate the sources we used (all units in cm):

- **Basic cube**: The centre coincided with the origin. Three sources were used: A at z = -2.04, B at z = 0 and C at z = 2.04, we point out that the Basic cube spread out from z = -2.54 (-1") to $z = 2.54$ (1").
- **Basic cuboid**: Here, the entry face coincided with the origin, while the rear face is at $z = 25.4$ (10"). Like the Basic cube, three sources were apportioned through the Basic cuboid: A at $z = 0.5$, B at z = 12.7 and C at z = 24.9.

[2] G4GeneralParticleSource
[3] 511 keV, 662 keV, 1.333 MeV, 5 MeV, 10 MeV, 20 MeV, 30 MeV, 40 MeV and 50 MeV

- **Phoswiches**: The phoswhiches' Cubes were positionned at the same place and had exactly the same three sources than the Basic cube: A at z = -2.04, B at z = 0 and C at z = 2.04. Regarding the rear Cuboid, it had five sources: D at z = 3.04, E at z = 6.6, F at z = 10.16, G at z = 13.72 and H at z = 17.28. The Cuboid began at z = 2.54 and ended at z = 17.78 (7").

The clarification of the sources coordinates is really important to ease the discussion on the results analysis. There will be clear features on some figures that will have a dependence on the sources location, as we will see, for example, in section 3.2.3. See figure 3.1 for a visual representation.

3.2.1 Efficiencies

It is important to measure the efficiencies not only to know where (in energy) our detector is performant, but also to help decide which photomultiplier will be used and how it shall be set for they have different sensibilities. We know the wavelength of emission (see figure 2.1), but in order to optimize the detection, we need to set a threshold on the optical photons number to eliminate as much background noise as possible. The knowledge of how the energy is absorbed gives us precious information about the real yielded scintillation light for each crystal.

As defined in the section 2.1.1, ϵ_{intr} is the fraction between the number of detected γ-rays and γ-rays entering the detector. This means that we do not need a realistic source for this measure since we would ignore the γ-rays emitted away from the detector anyway. In order to save computing time, we chose the cone beam for this efficiency measurement. Note that the cone diameter was equal to the face's diagonal, not the side length. This means that we had a little extra beam shoving off on each side, implying nothing more than a little geometry calculation to scale ϵ_{intr} (it is to be coherent with our analysis procedure where each γ-ray was considered as entering the detector). We can see the result in figure 3.3's top-left graph. At low energies, ϵ_{intr} almost reaches 100% then it quickly lowers to 45%, pulling up slowly afterward. This last feature is expected considering the different γ-matter interaction processes' cross section (see fig. 1.2).

We had two ways to determine the absolute efficiency ϵ_{abs}. We could either follow our definition and emit with a 4π source, or we could use the data coming from the conic beam and do a little calculation to get the same result. The latter's asset is the higher possible statistics for the same computing time. Of course, we will need to convolve the result with the solid angle. In fact, we will use the second definition given in section 2.1.1: we already measured ϵ_{intr}, so we only need to multiply it by ϵ_{geom}, which is the fraction of the solid-angle subtended by the detector face which was 5 cm apart from the source. This is why this curve, as seen in figure 3.3's top-right graph, has the same shape than ϵ_{intr}'s one: it was only multiplied by this fraction.

ϵ_{pp} and $\epsilon_{p/T}$ (respectively fig. 3.3's bottom-left and bottom-right graphs) were analyzed for four different cases: a full absorption without condition, a full absorption exclusively in the LaBr3, a full absorption exclusively in the NaI and the sum of the last two ones (respectively the black, the blue, the red and the green curves). The percentages are coherent with what we find for ϵ_{abs}. A low-energy γ-ray is fully absorbed in most cases, while it is quite different at high energies. We can also note that the NaI do not frequently fully absorbs on its own. This is no surprise since an incident γ-ray will more likely interact with the LaBr3 at least once before being fully absorbed by the NaI second layer. This does not mean that the NaI doesn't play a role in the full absorption spectrum. Indeed, the black curve is the highest, meaning that there are cases were an incident γ-ray will interact one or several times in the LaBr3 before ending its course in the NaI. It is true that this role is not that important for a single phoswich, still, we see a difference between the green and the black curves. In a cluster assembly, this role becomes more important because a high volume enables, among other, a better Compton scattering accounting. Indeed, the shower generated by a γ-ray interaction in the LaBr3 propagates not only toward the rear scintillator of the given phoswhich, but also in the neighboring ones.

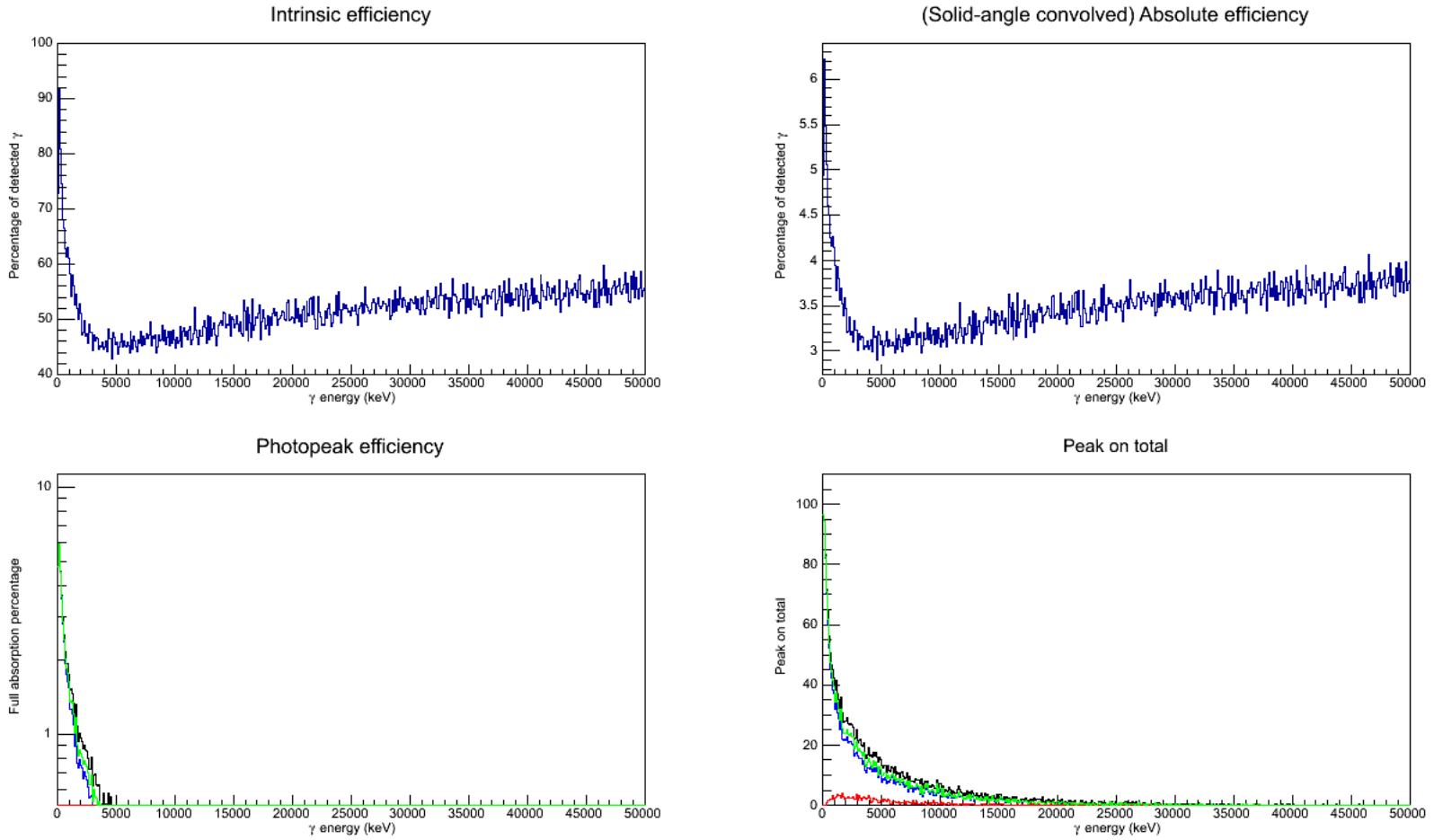

Figure 3.3: LaBr3\NaI Phoswhich efficiencies

Efficiency curves in percentage, depending on energies. For the efficiencies definition, see section 2.1.1. For the curves analysis, see section 3.2.1.

3.2.2 Signal

What we will be calling the "signals" corresponds to what an electronic acquisition would actually detect when a γ-ray hits the detector. As defined in section 2.2.2, each scintillator emits its light with a delay and the signal's shape is made of one or more exponential components. On figure 3.4, we can see two plots of such signals. Figure 3.4a is an experimental signal whereas 3.4b is a simulated one. Both plots were fetched the same way : the blue curve is the measured signal for a detector made of a LaBr3 cube, the red one is a NaI cube and the black one is what we detect for a NaI phoswich.

We had no electronic acquisition in our simulations, but we had the information on the optical photons lifetimes (time elapsed between the emission and the absorption). While the absolute figures between the experimental and the simulated results cannot be compared, we can however look closer at the shapes of the different plots. And it seems they exhibit similarities: all three have a faster LaBr3 signal and it is followed by the NaI. We have to specify that our materials were not parametered correctly regarding the risetimes. It was one nanosecond for each scintillator, whereas in reality each has a specific value.

We know that the speed of light in a given medium is $v = \frac{c}{n}$, with $c = 299\ 792\ 458\ m.s^{-1}$. Doing a little calculus gives us $v_{LaBr3} = 146.24\ mm.ns^{-1}$, $v_{NaI} = 162.05\ mm.ns^{-1}$ and $v_{CsI} = 168.42\ mm.ns^{-1}$. Let's take a mean speed of 160 $mm.ns^{-1}$. Typically, a photon will need 1.27 ns to cross a 8" phoswich, which is in the order of magnitude of the characteristic time components.

3.2.3 Optical photon analysis

An important part of our work was the study of the optical photons' behavior. In this section, we will be interested on where are the optical photons and how they travel through the scintillating crystals. These are important questions in order to better understand what are the determining parameters regarding the detection of the scintillation light at the photocathode. The simulations were done using a scanning configuration for the sources.

z distribution

Let's take a closer look at the absorption point. In figure 3.5, we plotted the number of absorbed optical photons against the z-coordinate of the absorption point in NaI and LaBr3, Specular and Lambertian phoswiches for 30 keV γ-rays sources. The results are similar with 662 keV sources, but the Compton scattering bothers us by adding an effect not useful to analyze this aspect. Note that the y-axis is on a logarithmic scale. In table 3.1, we show the percentages of optical photons absorption. The "lost" percentages refers to optical photons that either escaped through the reflector (3% of transmission probability) or that has been absorbed in the scintillators. Like we said, the quantum efficiency of the photocathode is set to 100%, so any optical photon reaching it is counted in the second percentage.

In figure 3.5, we first notice the higher count around $z = 180\ mm$. This is good news because the photocathode of a phoswich is at $z = 17.78\ cm$, meaning that much scintillation light is absorbed at the right place. Indeed, any optical photon not reaching the photocathode is lost and can't be accounted for on an experimental device. Looking at the table informs us that actually between one and two third of the optical photon number is lost, this is not negligible. An interesting question is what happens if we add an aluminimum casing ? Of course, the UNIFIED model implemented in GEANT4 simulate transmission for 3% of the optical photons in our case. But what happens exactly when transmission occurs ? Can a transmitted optical photon be reflected back in the scintillator when reaching the aluminimum ? What happens for Teflon surfaces ? These questions are yet to be answered, requiring a more realistic model (see the end of section 3.2.4).

In the NaI phoswiches, we can see two general shapes: one regrouping sources A and C with a high count, the other uniting sources D and G with a low count. This is explainable by the different scintillation yield of the two coupled crystals and this is why we do not see these shapes in a LaBr3 phoswich where the crystal for both components is the same. Indeed, the LaBr3 and the NaI respectively yield 63 000 photons/MeV and 38 000 photons/MeV.

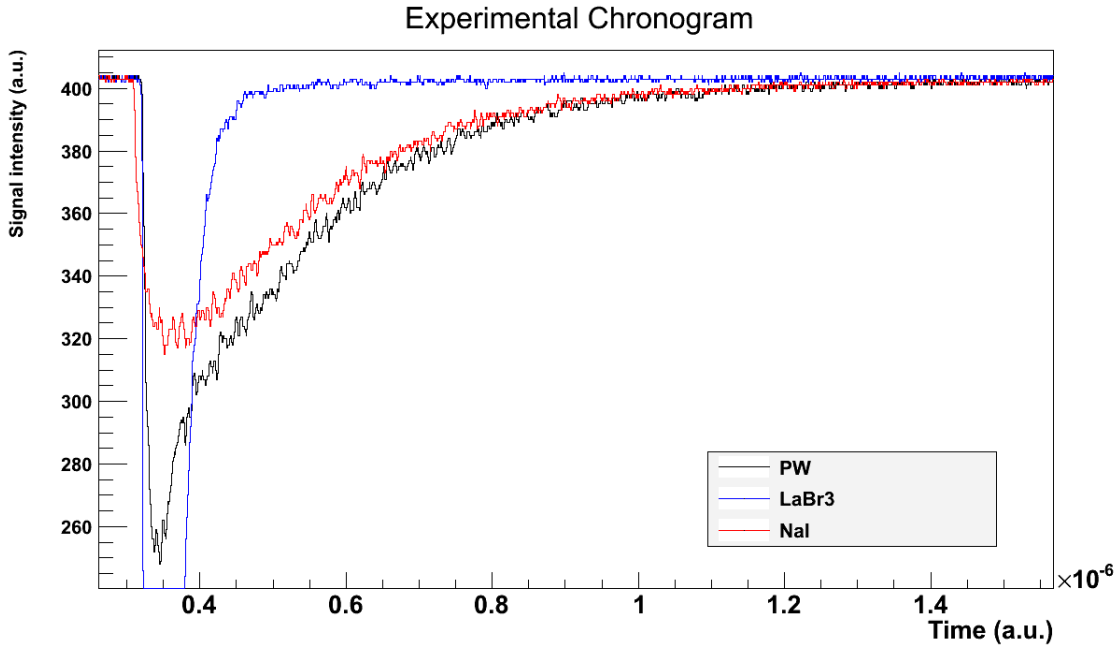

(a)

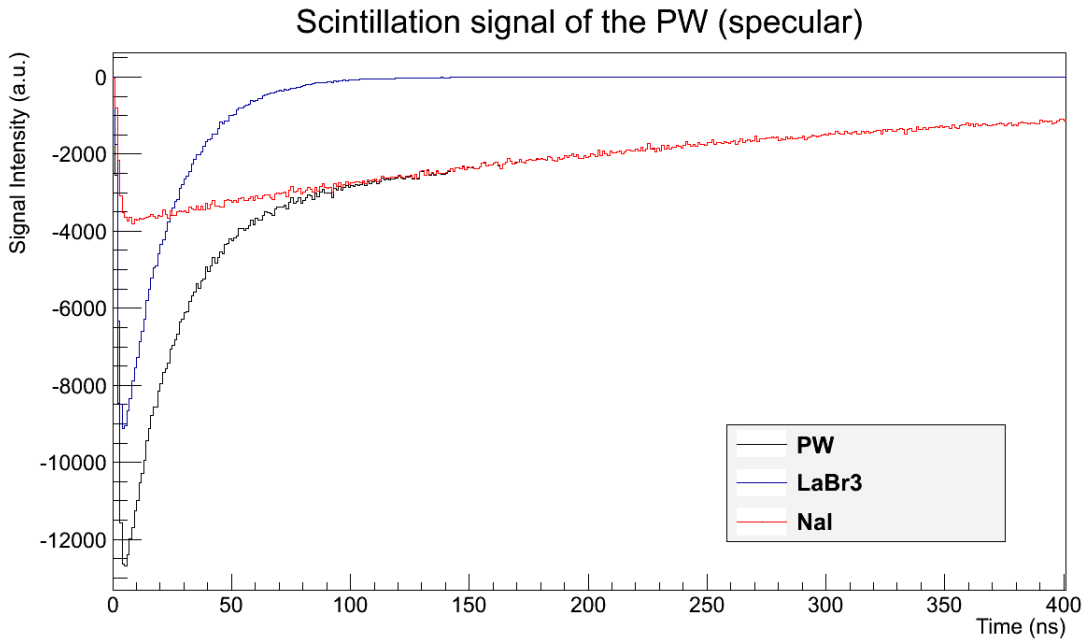

(b)

Figure 3.4: Signals
The top figure comes from experimental measurements while the other is a simulated signals.

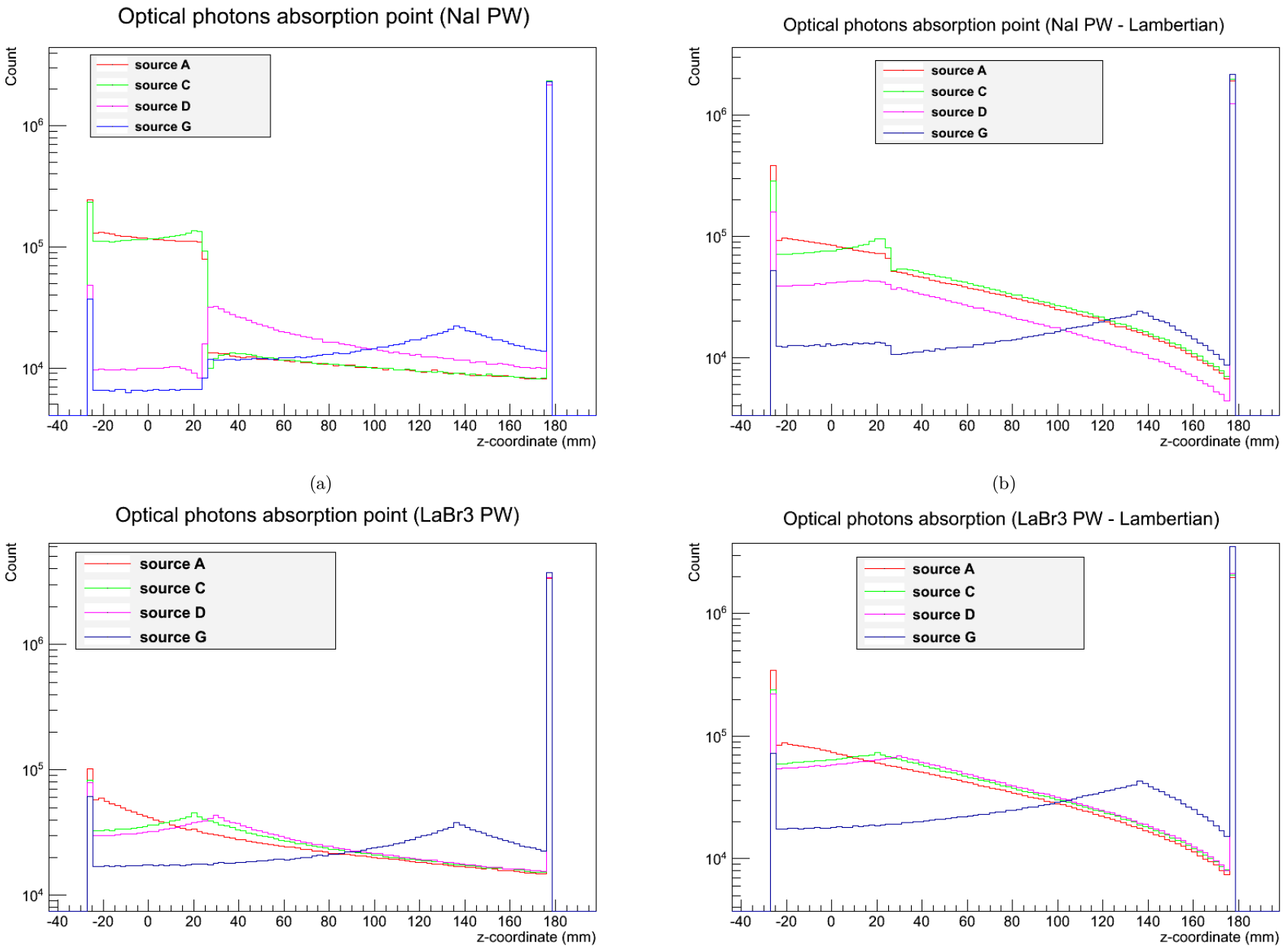

(a) (b)

(c) (d)

Figure 3.5: Optical photons absorption point for several phoswich configurations (LaBr3 or NaI - Specular or Lambertian)

Assembly	Source	Lost	Reaching Photocathode
Specular PW NaI	A	58.69 %	41.31 %
	C	58.59 %	41.41 %
	D	36.80 %	63.20 %
	G	32.13 %	67.87 %
Specular PW LaBr3	A	40.44 %	59.56 %
	C	39.92 %	60.08 %
	D	39.73 %	60.27 %
	G	34.22 %	65.78 %
Lambertian PW NaI	A	66.53 %	33.47 %
	C	65.38 %	34.62 %
	D	63.64 %	36.36 %
	G	37.29 %	62.71 %
Lambertian PW LaBr3	A	65.13 %	34.87 %
	C	63.70 %	36.30 %
	D	62.75 %	37.25 %
	G	37.67 %	62.33 %

Table 3.1: z distribution statistics, discussion in section 3.2.3.

Finally, we notice a mountain-shaped distribution for each source where the top of it coincides with the source z-position. It seems to be due to a trapping effect: for example, source G is at $z = 13.72\ cm$ and emits γ-rays toward the x-axis. When a γ-ray is absorbed, the yielded scintillation light is emitted in 4π, implying a few optical photons directed along the x-axis or the y-axis. What was unexpected is the similarity between the Lambertian and Specular reflectors. One could anticipate that a Lambertian reflector would wash out any structure of this kind because of the random reflections. As we can see, it is not the case. We will try to correlate these shapes with the trajectory lengths in the proper subsection. Another interesting avenue to explore is the polarization of the scintillation light influence. During our simulations, no input has been given for it and GEANT4 printed messages informing us of the assumed random polarization. It could be intriguing to see if a selection on the polarizations during data analysis would correlate these with the z-coordinate of the absorption points.

Photocathode patterns

Another interesting aspect to better understand the optical photons whereabouts is the study of what we call the photocathode patterns. These are slices of the detector taken at the photocathode entry face and representing the number of optical photons absorbed on each (x,y) point. The idea is to correlate the detected pattern with a given source's caracteristics. We ran several simulations on different geometries and checked the patterns out. All used sources emitted 30 keV γ-rays in the scanning configuration. Some of them were decentered[4] so that the awaited isotropy was broken, giving us a chance to find specific patterns.

The first case we studied was the basic Specular LaBr3 cube. We looked at the patterns for edge sources A, B and C: the results are in figure 3.6. Generally, we can see a higher count on the source's side, even for A. For source B, we can guess its position since there is a circular shape where the density is higher. This gets obvious for source C which is just beside the photocathode. We can follow a similar reasoning for the basic Lambertian LaBr3 cube (centered source, see figure 3.7). This is promising be-

[4]Two cases: "edge" for (x,y) = (-2.04,0) cm and "corner" for (x,y) = (-2.04,-2.04) cm

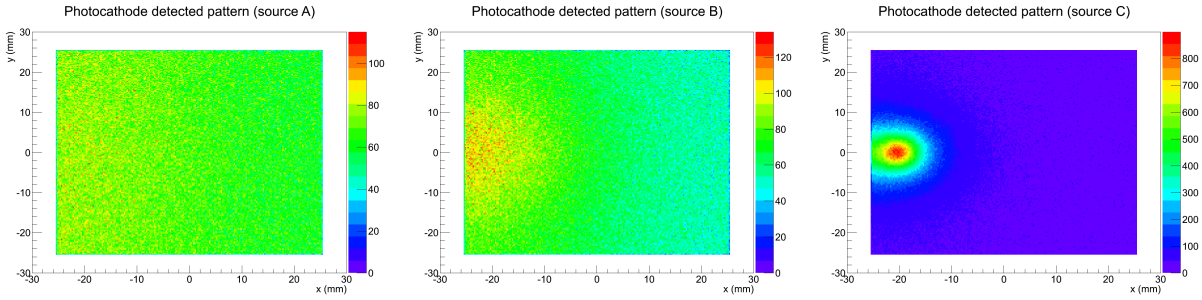

(a) (b) (c)

Figure 3.6: Photocathode patterns for the LaBr3 Specular cube, edge sources

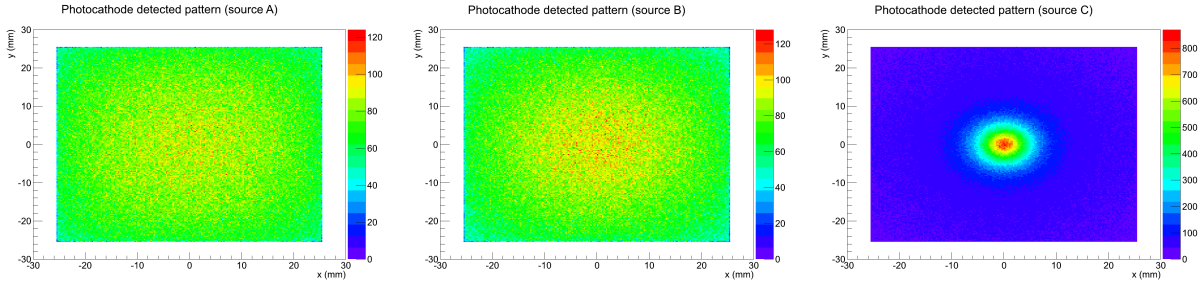

(a) (b) (c)

Figure 3.7: Photocathode patterns for the LaBr3 Lambertian cube, centreed sources

cause it suggests that we can learn something on the interaction point position only by looking at the pattern.

In our study, this only worked for the LaBr3 cube. Whenever the depth of the detector was increased, we lost this kind of pattern shape and it was even more washed out with a phoswich (see figure 3.8 and 3.9). All the following results are similar: it does not seem that we can extract any information using the pattern for anything else than a basic cube. The main issue here is that we want to have a high volume to increase the efficiencies, but as the depth augments, we lose any pattern.

Trajectories length

Always using 30 keV γ-rays, we plotted the optical photons trajectory lengths, meaning the distance they traveled between their emission and absorption point. The results are quite satisfactory and concord with the phoswich geometry. Indeed, when we look closer at the Specular case (figure 3.10a), say for

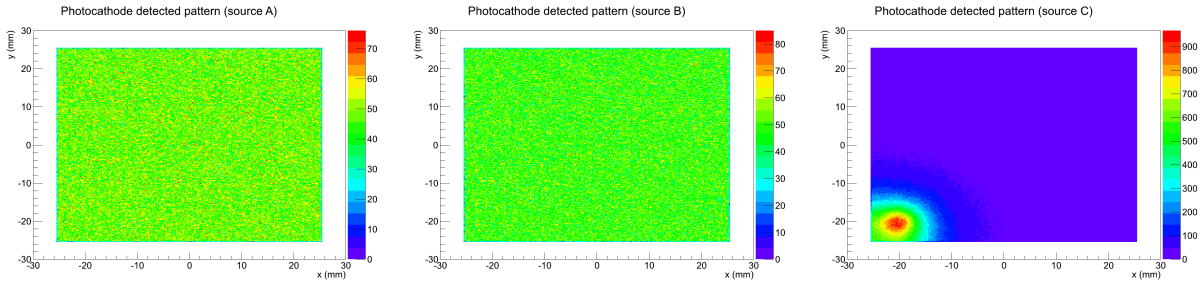

(a) (b) (c)

Figure 3.8: Photocathode patterns for the LaBr3 cuboid, cornered sources

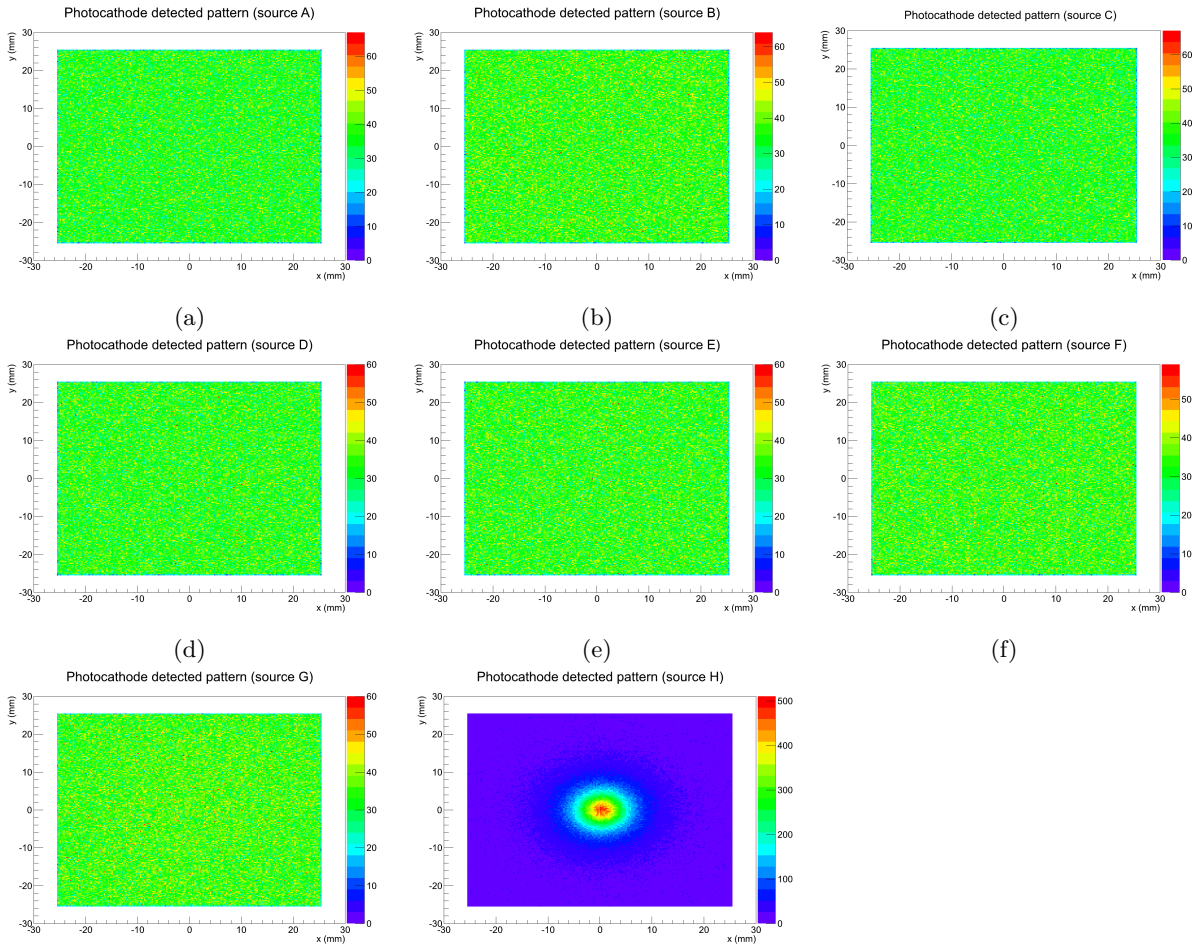

(a) (b) (c)

(d) (e) (f)

(g) (h)

Figure 3.9: Photocathode patterns for the NaI PW, centreed sources

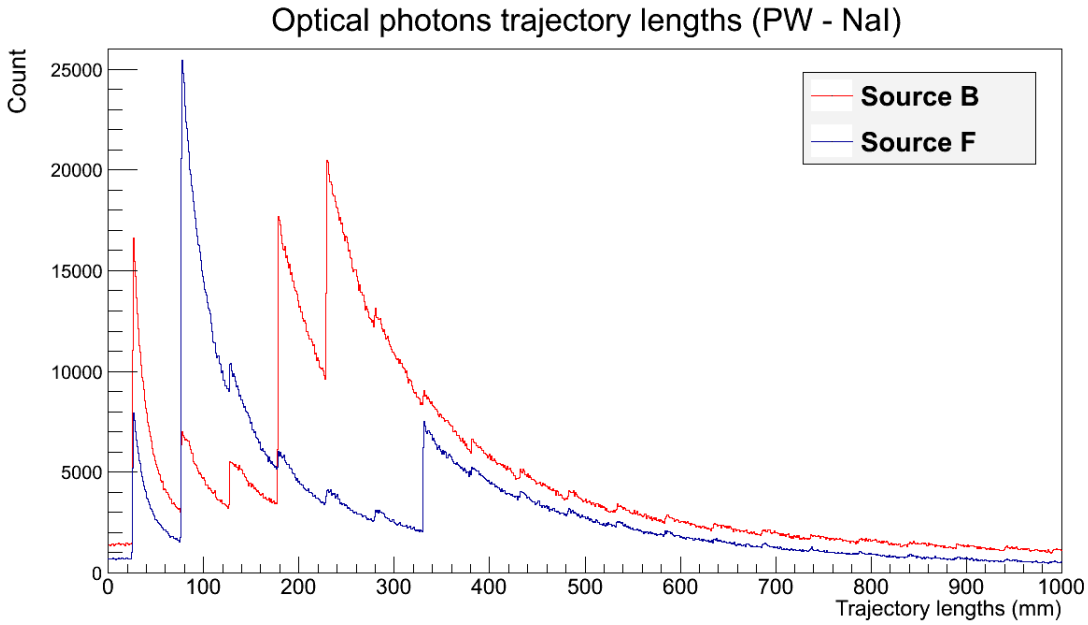

(a)

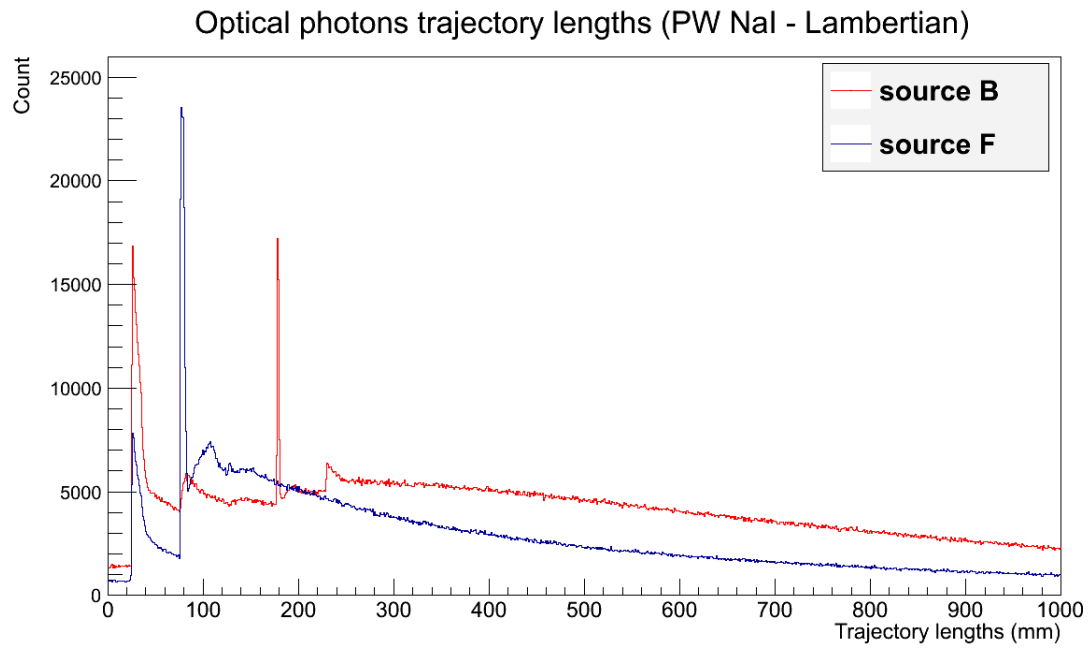

(b)

Figure 3.10: Optical photons trajectory length in NaI phoswiches (Specular and Lambertian) for 30 keV γ-rays

source B, we notice a first peak at $x = 26\ mm$. This corresponds to 1", which is the distance with the nearest edge (for this source, in any unit vector direction). The slow decrease afterwards is to be associated with increasing angles (the higher the angle, the longer the trajectory). Starting at this first peak, we periodically have other peaks every two inches. Of course, when a normal optical photon reaches an edge, it is reflected back and travels two inches toward the next edge when parallel to either the x-axis or the y-axis. Between each peak, we see the decrease already spoken of. We then reach two high peaks respectively at $x = 180\ mm$ and $x = 230\ mm$. These are the first optical photons absorbed by the photocathode. The source B is at $z = 0$ and the photocathode is at $z = 17.78\ cm$ in such a configuration. The second high peak is the optical photons emitted from source B toward the negative z-axis. After travelling 1" + 1" to the entry face, they follow the same trajectory than the one in the first high peak. This reasoning is totally applicable for source F. It is positionned at $z = 10.16\ cm$ and the highest peak is at $x = 76\ mm$: $10.16 + 7.6 = 17.76\ cm$, the z-coordinate of the photocathode.

The Lambertian curves are quite different. First, there are less noticeable peaks, only two really outstrip the others. They do have characteristics length: for source B (always at $z = 0$), the first peak is again at 1", which corresponds to the first edges' reach (in either x, y or z direction). The second one is at 7", which is the distance between the source and the photocathode. Same reasoning for the F source.

We can conclude on the trapping effect we mentionned in the z distribution section. We do see absorption peaks every two inches in the Specular case. In the Lambertian case, we see a high peak at 1", which is to be associated with the top of the moutain (see z distribution section) and a continous distribution, explaining the wider moutain for this case.

3.2.4 Resolution

As defined in section 2.1.2, the resolution corresponds to the $\frac{\Delta E}{E}$ ratio. What happens in reality, is that we do not detected an energy directly, but an optical photon number. Knowing the scintillation yield of a given material, we can retrieve the energy by counting the optical photons and correctly calibrating our detector beforehand with a known source. This implies that discussing the resolution should be discussing on the detected scintillation photons number. The scanning configuration was used for the sources since the experimental data was fetched with a collimated source.

Let's first take a look at figure 3.11. Both plots are the number of optical photons detected at the photocathode depending on the source position. The top figure presents the experimental results of J. Peyré *et al.* [16] whereas the bottom one shows the results of our simulations. Note that the x-axis is reversed for the two graphs: the upper one is the distance to the photocathode, while it is the z-coordinate for the lower one, the photocathode being at the highest z-coordinate for the latter. The configurations in both cases were not the same. Although the used source in the experiment was of the same energy than ours[5], the geometries were a little bit different. The experimental LaBr3 generally had a cuboid shape (except for one cylinder), while we had a cube. Moreover, the geometries were thiner for the phoswiches (we had 2" × 2" × (2" + 6") while they had 1" × 1" × (2" + 6")). This difference is important at 662 keV because we anticipate a higher optical photon loss due to more reflections and a higher Compton scattering effect (less interaction volume).

The first discrepancy that we may note is that in simulations on phoswiches, the count for the LaBr3 component is higher than for the NaI or CsI one. It is the opposite in the experimental data. We may conceive that the geometry is responsible for this, as we already mentionned above. We see other dissimilarities on the statistics. Comparing table 3.2 data with the percentages of the experimental plot, we see numerous differences. For example, we are interested in the LaBr3 resolution loss when appended to a phoswich. The experiment shows that the loss ratio is $\frac{3\%}{3.79\%} = 79.16\%$, while the simulation yields $\frac{3\%}{4.33\%} = 69.28\%$ for a NaI phoswich. In the CsI phoswich case, we have $\frac{3\%}{4.51\%} = 66.52\%$ for the experiment and $\frac{3\%}{4.59\%} = 65.36\%$ for the simulation, which is more comparable[6]. Again, the models differences may account for this and although the results are not the same, they stay quite near from each other.

[5] a 662 keV γ-ray coming from a ^{137}Cs source

[6] One should remind that in our work the scintillation yield for the CsI crystals were not realistic.

We also clearly see a lower resolution with the CsI phoswich, explainable by the trapping effect due to the higher optical index difference between the CsI and the LaBr3 than between the NaI and the LaBr3. Indeed, an optical photon reaching an interface between two different optical-index media will have a probability of being reflected back. We have a third discrepancy regarding the inhomogeneities. Always comparing the table with the figures on the experimental plot, we note that there are no inhomogeneities for the experimental stand-alone LaBr3 crystals while the phoswiches do have a standard deviation. Our simulations always yield non zero standard deviation.

An observable similarity is that the LaBr3-only assemblies are above the phoswiches made of different scintillating materials in both cases. More precisely, there is about a factor 2 in the counted optical-photons or photo-electrons between the stand-alone LaBr3 cube or cuboid and the NaI or CsI phoswiches in both cases.

The PARIS collaboration made other measurements with phoswiches of the same size than ours, and the experimental data yields a LaBr3 resolution from 4.2% to 4.8% when in a phoswich assembly. Calculating the loss ratio, we find $\frac{3\%}{4.2\%} = 71.43\%$ to $\frac{3\%}{4.8\%} = 62.50\%$ compared to the simulated result which is 69.28%. With the same geometries, the simulations and the experiments are in fair agreement.

We continue our analysis using figure 3.12 and the two arrays of table 3.2. We are still in the 662 keV γ-ray case, but we added the Lambertian results to our Specular curves. We immedialy see the higher standard deviation for the Lambertian curves, both in the table and on the plot. We were surprised by such shapes, always thinking that a 2π reflection would flatten any special feature. We see that the Lambertian curves are initially lower that the Specular ones for each respective setting, getting higher about source G position. In other words, the Lambertian surface seems more efficient when near from it, while the Specular reflector appears more adapted when far from the rear. More work is needed on this feature too. At this stage, these results do not explain why St-Gobain, which construct the phoswiches, uses Lambertian surfaces (at least, they told us that it is Lambertian in a first approximation [17]). Of course, it is probably a better reflector, but in order to correctly compare with experiment, we need a full description of the reflectors and of the phoswich components. The access to these informations is not always easy since St-Gobain protects its industrial secrets. Even if we had these informations, we need to implement them in our simulations. We must remember that our models are basic with only a defined material for each scintillator, a reflector and a perfect photocathode. In reality, we need to add components like a more realistic entry face, a "window"[7] between the two scintillators, a realistic reflector, the "window" between the rear scintillator and the (more realistic) photocathode or optical glue between each component.

[7] knowing the exact matter being used

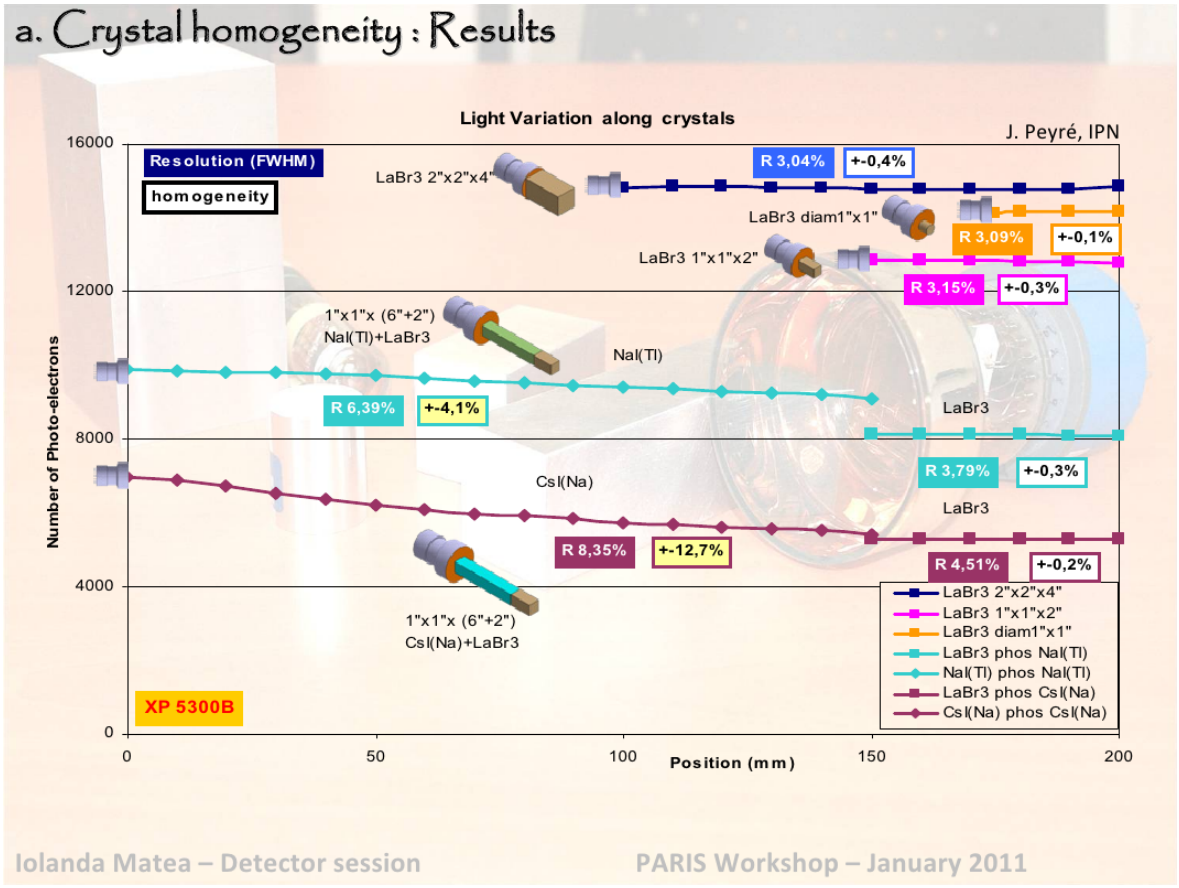

(a)

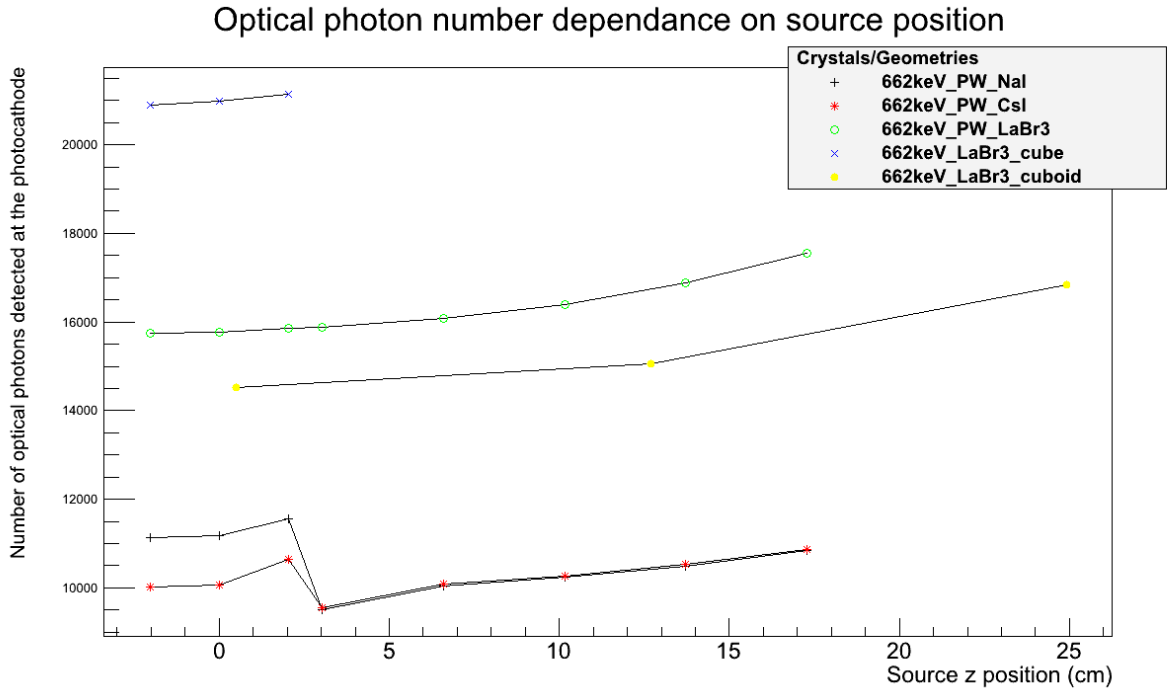

(b)

Figure 3.11: Optical photon number reaching the photocathode: simulated vs experimental

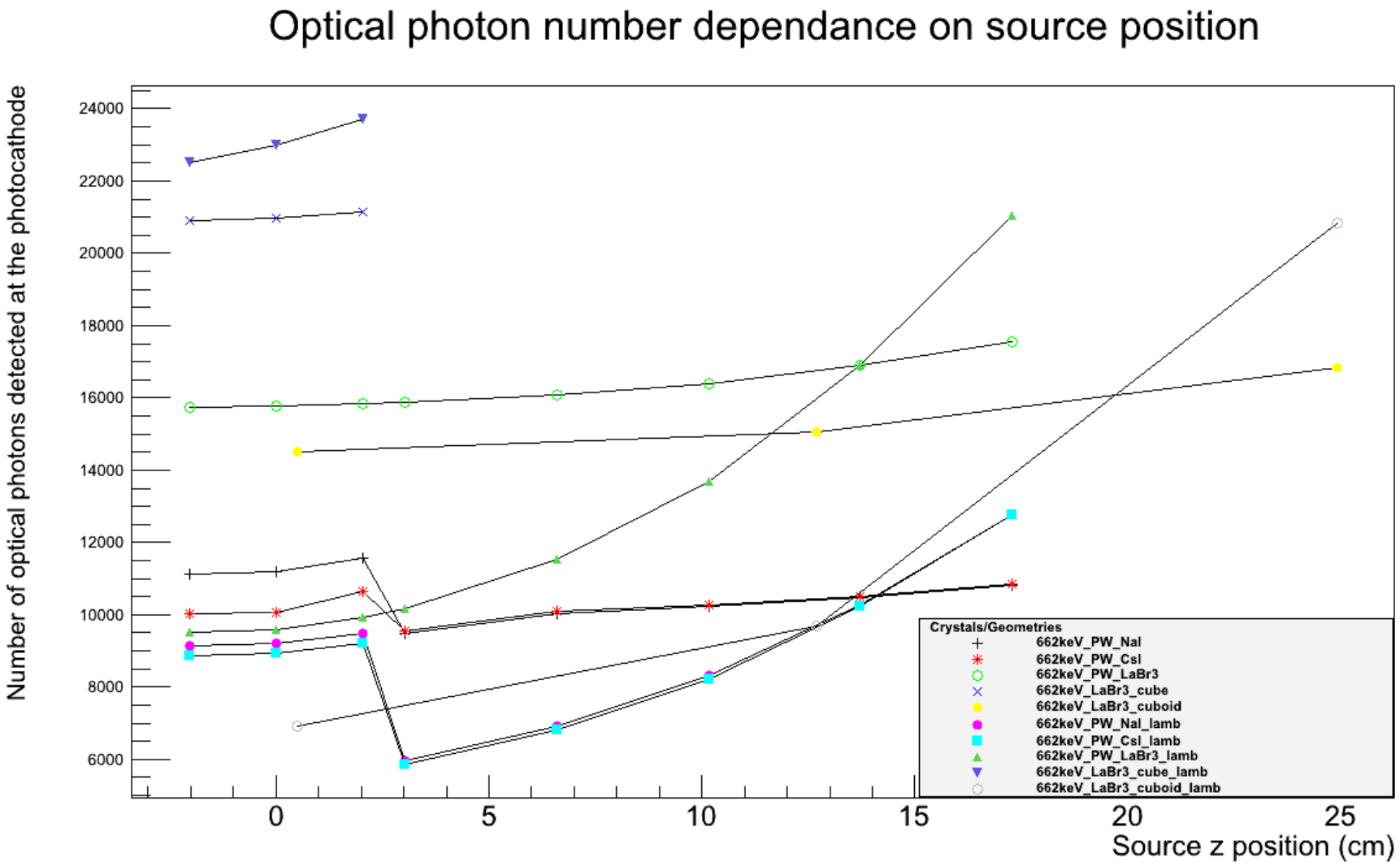

Figure 3.12: Simulated data: Specular vs Lambertian at 662 keV

662 keV - Specular

Assembly	**Block**	**Mean Resolution**	**Optical photon number Standard deviation**
PW NaI	LaBr3 cube	4.33 %	1.71 %
	NaI cuboid	6.81 %	4.38 %
PW CsI	LaBr3 cube	4.59 %	2.82 %
	CsI cuboid	6.87 %	4.26 %
PW LaBr3	LaBr3 cube	3.51 %	0.29 %
	LaBr3 cuboid	3.43 %	3.65 %
Cube	LaBr3 cube	3.00 %	0.52 %
Cuboid	LaBr3 cuboid	3.54 %	6.39 %

662 keV - Lambertian

Assembly	**Block**	**Mean Resolution**	**Optical photon number Standard deviation**
PW NaI	LaBr3 cube	4.91 %	1.62 %
	NaI cuboid	7.38 %	27.55 %
PW CsI	LaBr3 cube	5.10 %	1.57 %
	CsI cuboid	7.37 %	28.21 %
PW LaBr3	LaBr3 cube	4.52 %	1.88 %
	LaBr3 cuboid	4.25 %	26.72 %
Cube	LaBr3 cube	3.01 %	2.16 %
Cuboid	LaBr3 cuboid	3.60 %	48.19 %

Table 3.2: Mean Resolution and Standard deviation of the optical photon number reaching the photocathode

Conclusion

"Why is this effect worse for a specific scintillator than another ? Why is there a different detection inhomogeneity for different cristals ?"

We started this report with these questions. Our study is to be seen as a beggining of the trails exploration and in order to fully answer these questions, we need to go all the way in those tracks. Nevertheless, work was done and we have part of the answers.

After presenting the context around the PARIS collaboration which falls within the SPIRAL2 project, we reminded the γ-matter interaction processes: the photoelectric effect, the Compton scattering and the pair production. We then went around detector theory, starting with the definitions of four efficiencies and the resolution and continuing with inorganic scintillators specificities: theory on the scintillation process, the specific detected signal shape of a scintillator and the utilized physical assemblies.

Our results were finally analyzed. We started with the presentation of our simulations' setup (both used assemblies and sources). We then studied several aspects of our simulated data. We found that the efficiencies were way better at low energy, especially for the first block (LaBr3) in a phoswich. The usage of a NaI cuboid on the rear of the phoswiches enabled us to augment the detection volume and this was particularly true in cluster assembly (3×3 phoswiches), since it better took into account the showers coming from the Compton scattering or the pair production. The signal shape study showed an agreement between experimental and simulated data. We pursued with three points regarding the optical photon analysis: the z distribution of the absorption point, the photocathode patterns and the trajectory lengths. The z distribution study gave us percentages of optical photons loss, which were quite high (between one and two thirds). A closer look at the photocathode patterns, with the hope of learning something on the detection point, were inconclusive except for a small LaBr3 cube. The trajectory lengths, in turn, partially explained the moutain-shaped peaks of the z ditribution and fairly accounted for our detector geometries. Finally, we checked out the resolutions statistics on the optical photon count at the photocathode. We were again in agreement with experimental data with a LaBr3 resolution degradation of about 1.2%.

The important point to remember is that our models could be more realistic. Our phoswiches were made of two scintillators and a perfect photocathode, surrounded with "pseudo-air", while in reality the assembly is more complex and features at least two times more components, though information is sometimes hard to get because of industrial secrets. Same thing for the CsI we used: it had an unrealistic scintillation yield since, as a first step, we were only interested in the effect of the optical index change comparing to the NaI and the LaBr3.

Bibliography

[1] "Ganil-spiral2 website." http://www.ganil-spiral2.eu/spiral2-us/scientific-advances.

[2] A. Maj et al., "The PARIS Project," *Acta Physica Polonica*, 2009.

[3] C. le Sech and C. Ngô, *Physique Nucléaire, des Quarks aux Applications*. Dunod, 2010.

[4] "Xcom: Photon cross sections database." http://www.nist.gov/pml/data/xcom/index.cfm.

[5] C. Theisen, *Excitations multiparticules dans le noyau superdéformé* ^{1}49 *Gd. Signature d'une symétrie nouvelle* C_4 *du noyau*. PhD thesis, Centre de Recherches Nucléaires Strasbourg, 1995.

[6] W.R.Leo, *Techniques for Nuclear Particle Physics Experiments*. Springer-Verlag, 1994.

[7] "Saint-gobain website." http://www.detectors.saint-gobain.com/Phoswich.aspx.

[8] C. L. Melcher, "Scintillation crystals for pet," *The Journal of Nuclear Medicine*, 2000.

[9] Photonis, *Photomultiplier Tubes - Principles and Applications*. Photonis, 2002.

[10] C. Amsler, D. Grögler, W. Joffrain, D. Lindelöf, M. Marchesotti, P. Niederberger, H. Pruys, C. Regenfus, P. Riedler, and A. Rotondi, "Temperature dependence of pure csi: scintillation light yield and decay time," *Nuclear Instruments and Methods in Physics Research Section A*, 2002.

[11] J. Birks, *The theory and Practice of Scintillation Counting*. Pergamon Press Ltd., 1964.

[12] M. Fox, *Optical Properties of Solids*. Oxford University Press, 2010.

[13] A. Levin and C. Moisan, "A more physical approach to model the surface treatment of scintillation counters and its implementation into detect," *TRIUMF Preprint TRI-PP-96-64*, october 1996.

[14] O. Stézowski, "La spectroscopie gamma : des faisceaux stables aux faisceaux radioactifs." Habilitation à Diriger des Recherches, 2008.

[15] "Refractive index database website." refractiveindex.info.

[16] J. Peyré and I. Matea. Private communication.

[17] S.-G. P. Plastics. Private communication.